

1  
2 **Serpentinites of Different Tectonic Origin in an Exhumed Subduction Complex (New**  
3 **Caledonia, SW Pacific)**  
4

5 **Natalie H. Raia<sup>1</sup>, Donna L. Whitney<sup>1</sup>, Christian Teyssier<sup>1</sup>, Stéphane Lesimple<sup>2</sup>**

6 <sup>1</sup>Department of Earth & Environmental Sciences, University of Minnesota, Minneapolis, MN  
7 55455, USA.

8  
9 <sup>2</sup>Service Géologique de la Nouvelle-Calédonie, Direction de l'Industrie, des Mines et de  
10 l'Énergie, BP M2 – 98849 Nouméa CEDEX, New Caledonia.

11  
12 Corresponding author: Natalie Raia ([raia0003@umn.edu](mailto:raia0003@umn.edu))

13 **Key Points:**

- 14 • Two compositionally-distinct types of serpentinites identified in the New Caledonia  
15 subduction complex
- 16 • Some serpentinites derive from the subducting plate; others from the overlying mantle  
17 wedge
- 18 • New Caledonia preserves evidence for incorporation and exhumation of mantle  
19 hangingwall via the subduction channel
- 20  
21

**22 Abstract**

23 Owing to the importance of serpentinites for planetary geochemical and geodynamic  
24 processes, there has been much work discerning the origins of their parent rocks, including  
25 distinguishing between serpentinites derived from a subducting plate vs. overlying mantle in  
26 exhumed subduction complexes. The island of New Caledonia (SW Pacific Ocean) provides a  
27 rare window into Cenozoic Pacific subduction processes. The island is unique in exposing both  
28 an exceptionally-preserved high-pressure, low-temperature subduction complex and one of the  
29 largest supra-subduction zone ophiolites in the world. Previous studies disagree on the origin of  
30 serpentinites in the subduction complex. In this study, we analyze twenty-three serpentinites  
31 from this subduction complex for whole-rock major and trace element geochemistry and stable  
32 isotope ( $\delta D$ ,  $\delta^{18}O$ ) compositions. Our data reveal two distinct groups of serpentinites: Group I  
33 samples in the northern portion of the complex are pervasively serpentinized, and exhibit  
34 enriched heavy rare earth element (REE) compositions and  $\delta^{18}O$  between +6.7‰ and 10.2‰. In  
35 contrast, Group II serpentinites in the south preserve relict orthopyroxene and olivine, and show  
36 depleted trace element compositions and comparatively lower  $\delta^{18}O$  values between +5.1‰ and  
37 +8.0‰. We interpret Group I serpentinites to derive from downgoing plate mantle, whereas  
38 Group II serpentinites derive from overlying mantle wedge, exhibiting remarkable similarity to  
39 the REE geochemistry of the structurally-overlying New Caledonia ophiolite. Our results  
40 establish the subduction complex in New Caledonia as an unusual natural record of the  
41 entrainment and exhumation of mantle from both the overlying mantle wedge and the  
42 downgoing plate in an oceanic subduction zone.

**43 Plain Language Summary**

44 The hydration of Earth's mantle produces rocks called serpentinites that are important to  
45 chemical cycling within the Earth system. This process, a form of metamorphism, occurs in  
46 several types of tectonic settings on Earth. Serpentinites formed in these different settings are  
47 imparted with unique geochemical "fingerprints" due to different types of fluids and varied  
48 compositions of the original mantle material. In metamorphic complexes that preserve remnants  
49 of subduction zones, serpentinites can offer clues to the original tectonic setting and subsequent  
50 mechanics of subduction. We analyze stable isotope and whole-rock compositions to determine  
51 the origin of the mantle that produced serpentinites found in the metamorphic complex preserved

52 in New Caledonia (SW Pacific). We discover two distinct groups of serpentinites: one group in  
53 the northern portion of the complex likely formed on the ocean floor prior to subduction, and  
54 experienced high degrees of fluid alteration as it was metamorphosed. In contrast, a second  
55 group of serpentinites in the southern portion of the complex resembles material from the mantle  
56 overlying the subducting plate and is less altered. This locality represents an uncommon  
57 example, globally, where material from this overlying mantle is entrained and preserved at the  
58 surface in an exhumed subduction complex.

## 59 **1 Introduction**

60 Serpentinites are hydrated fragments of Earth's mantle and commonly occur in exhumed  
61 subduction complexes. They are important vehicles in the global cycling of water, carbon,  
62 nitrogen, fluid-mobile elements (FME), and halogens, releasing these elements by prograde  
63 dehydration at forearc to subarc depths during subduction (e.g., Alt et al., 2013; Barnes et al.,  
64 2018; Collins et al., 2015; Deschamps et al., 2011; Halama et al., 2014; Hattori & Guillot, 2003;  
65 John et al., 2011; Kerrick & Connolly, 1998; Kodolanyi et al., 2012; Scambelluri et al. 2004,  
66 2019; Tenthoey & Hermann, 2004; van Keken et al., 2011). Serpentinites and their hybridized,  
67 metasomatized derivatives formed at depth in subduction zones are critical in producing the  
68 distinct chemical composition of arc magmas (e.g., Codillo et al. 2018; Hattori & Guillot, 2003;  
69 Marschall & Schumacher, 2012; Nielsen & Marschall, 2017; Shimoda & Kogiso, 2019; Tatsumi,  
70 1986) and contribute significantly to the net redox budget of subducted oceanic plates and the  
71 oxidation state of dehydration fluids infiltrating the overlying mantle (Debret & Sverjensky,  
72 2017; Evans, 2012; Evans & Frost, 2021; Evans et al., 2017). The wide stability field of the  
73 serpentine mineral antigorite also makes possible the transport of these chemical components  
74 deeper into the mantle, past subarc depths (e.g., Hacker, 2008; Hattori & Guillot, 2003; Kendrick  
75 et al., 2011, 2017; Scambelluri & Tonarini, 2012; Schmidt & Poli, 1998; Ulmer & Tromsdorff,  
76 1995; Wunder & Schreyer, 1997).

77 Serpentinites are also critical to the rheology of the subducting zone, and in particular the  
78 plate interface (Gerya et al., 2002; Hermann et al., 2000; Rüpke et al., 2004; van Keken et al.,  
79 2011). Their high water contents and low density facilitate the exhumation of denser blueschist  
80 and eclogite (Guillot et al., 2000; Magott et al., 2020; Schwartz et al., 2001), and serpentinization  
81 of the cold "nose" of the mantle wedge carries implications for mantle wedge flow and the

82 minimum depth of decoupling of the subducting plate and overlying mantle (Hilairt & Reynard,  
83 2009; Kerswell et al., 2021; Reynard, 2013; Wada et al., 2008). Furthermore, serpentinites have  
84 been correlated with zones of slow slip and intermediate-depth seismicity in subduction zones,  
85 possibly associated with dehydration embrittlement resulting from the breakdown of antigorite  
86 (Behr & Bürgmann, 2021; Ferrand, 2019; Hacker et al., 2003; Hilairt et al., 2006, 2007; Hirth &  
87 Guillot, 2013; Jung & Green, 2004; Peacock, 2001; Proctor & Hirth, 2015; Toffol et al., 2022).  
88 In short, the occurrence, composition, and spatial distribution of serpentinites and associated  
89 metasomatic rocks in paleo-subduction complexes reveals information about first-order  
90 subduction processes, including the transport and chemical evolution of fluids during subduction  
91 and exhumation.

92 In exhumed subduction complexes, mantle material may originate from the downgoing  
93 plate or the overriding plate (Figure 1). Prior to subduction, serpentinites form in the (eventual)  
94 downgoing plate via hydrothermal circulation at ridge-transform systems where lithospheric  
95 mantle underlying the igneous oceanic crust or exposed at/near the seafloor by extension is  
96 hydrated by heated seawater (Barnes & O'Neil, 1969; Bonatti, 1976; Cannat, 1993; Cannat et al.,  
97 2010; Mével, 2003; Rouméjon et al., 2015). Hydration may also occur as the plate approaches  
98 the trench, if water circulates through slab-bend faults (Ranero et al., 2003). In the overriding  
99 plate, the mantle wedge experiences hydration from fluid fluxing off the dehydrating downgoing  
100 plate (e.g., Bostock et al., 2002; Fyfe & McBirney, 1975; Hyndman & Peacock, 2003).

101 Serpentinites formed in each of these distinct tectonic settings are geochemically distinct  
102 owing to differences in (1) mantle protolith composition (i.e., melt depletion and refertilization  
103 histories and degrees of fractional crystallization) and (2) the chemistry and nature of fluid  
104 alteration, such as fluid-rock ratio and temperature of serpentinization (Figure 1) (e.g.,  
105 Deschamps et al., 2010, 2013; Peters et al., 2017). These distinctions are evident in bulk-rock  
106 major and trace element geochemistry, stable isotopes (e.g., O, H, Cl, B), and the composition of  
107 relict primary minerals (e.g., spinel, pyroxene, and/or olivine) and have been proposed to be  
108 diagnostic of the tectonic setting of serpentinization. This has unlocked opportunities to discern  
109 the tectonic setting of mantle material exhumed in subduction complexes (Deschamps et al.,  
110 2010, 2013; Peters et al., 2017).

111 Studies aiming to determine the tectonic source of formerly subducted serpentinites must  
112 grapple with a nuanced, multi-staged history of serpentinization associated with pre-subduction  
113 processes and the prograde and retrograde paths of subduction and exhumation (Figure 1).  
114 Quantitatively determining the pressure ( $P$ ), temperature ( $T$ ), and time ( $t$ ) conditions experienced  
115 by exhumed serpentinites is challenging owing to high-variance phase assemblages, though  
116 promising new approaches expand options for unlocking both temperature and time in these  
117 rocks (Cooperdock & Stockli, 2016; Schwartz et al., 2020).

118 Complexities notwithstanding, there is a growing body of literature with examples of  
119 provenance interpretations of serpentinites in exhumed subduction complexes, such as studies  
120 assigning serpentinite associated with blueschist and eclogite to the downgoing plate (e.g.,  
121 Cooperdock et al., 2018; Katzir et al., 2000; Li et al., 2004; Scambelluri et al., 1991; Shen et al.,  
122 2015). Some studies have further resolved detail within the oceanic realm of the protolith,  
123 interpreting exhumed serpentinites to derive from passive margin settings (e.g., Barnes et al.,  
124 2014) or from abyssal transform faults (e.g., Cárdenas-Párraga et al., 2017). In many cases,  
125 however, non-distinctive geochemical signatures, lack of relict phases, and heterogeneity of the  
126 analyzed samples makes this level of resolution untenable. In other regions, the capturing of  
127 hangingwall mantle via subduction erosion and other mass transfer mechanisms has been  
128 identified (e.g., Bhat et al., 2019; Guice et al., 2021; Hattori et al., 2010; Lazar et al., 2021; Li et  
129 al., 2018; Tewksbury-Christle et al., 2021; Wu et al., 2018). In yet other localities, serpentinites  
130 from both the downgoing slab and the overlying mantle wedge are interpreted to be present,  
131 implying complex slab-mantle interactions at a range of depths (e.g., Barnes et al., 2013; Blanco-  
132 Quintero et al., 2011). These results generate discussion of deep tectonic slicing of slabs at depth,  
133 degrees of mechanical mixing and styles of deformation (e.g., coherent nappe stacking, block-  
134 and-matrix shear zones), and the processes of underplating and interaction with the mantle  
135 material of the overriding plate.

136 In this contribution, we discern the tectonic origin and alteration histories of serpentinites  
137 entrained in an Eocene high-pressure / low-temperature (HP/LT) subduction complex on the  
138 island of New Caledonia (SW Pacific) and explore implications for the subduction and  
139 exhumation history of the complex. The island of New Caledonia exposes an extraordinarily  
140 complete Eocene subduction-obduction complex, including a high-temperature metamorphic  
141 sole representing incipient stages of subduction initiation, an HP/LT subduction complex, and an

142 obducted supra-subduction zone ophiolite sequence (Maurizot et al., 2020a). These entities are  
143 well-studied and world-class sites: the ophiolite comprises one of the world's largest continuous  
144 mantle exposures and has provided invaluable insights into upper mantle processes and melt  
145 transfer in the lower crust (e.g., Cluzel et al., 2016; Dupuy et al., 1981; Marchesi et al., 2009;  
146 Pirard et al., 2013; Secchiari et al., 2016, 2018; Ulrich et al., 2010). The subduction complex  
147 exposes slivers of oceanic and thinned continental lithosphere that experienced blueschist and  
148 eclogite-facies metamorphism and has served as a location for investigation of subduction zone  
149 fluid-rock interaction, volatile recycling, and slab-mantle interactions (e.g., Cluzel, 2021;  
150 Spandler et al., 2008; Taetz et al., 2016, 2018). Despite the geodynamic importance of mantle  
151 rocks throughout the subduction-obduction complex, studies addressing the distribution,  
152 structure, texture, or geochemistry of meta-ultramafic rocks in the HP/LT complex are few  
153 (Cluzel, 2021; Fitzherbert et al., 2004; Rawling & Lister, 2002; Spandler et al., 2008). These  
154 studies arrive at differing conclusions regarding the source of the ultramafic material entrained in  
155 the complex. To evaluate these differences and determine the tectonic provenance and  
156 petrogenesis of ultramafic rocks in this subduction complex, our approach integrates field  
157 observations, petrographic characterization, whole rock major and trace element geochemistry,  
158 and stable isotope (O and H) geochemistry. Our results reveal the existence of two distinct  
159 groups of serpentinites, which we interpret to indicate differing tectonic settings for their  
160 protoliths.

## 161 **2 Geologic History of New Caledonia**

162 Located in the SW Pacific Ocean, the main island of New Caledonia exposes a dense  
163 array of geologic terranes that record Paleozoic and Mesozoic histories through to present day: a  
164 material archive that stands in contrast to many other islands in the Pacific, which are mostly  
165 entirely Cenozoic in age and volcanic in origin (Cluzel et al., 2012; Maurizot et al., 2020a; Paris,  
166 1981). The island (~16,000 km<sup>2</sup>) is a rare emergent portion of the NW-SE trending submarine  
167 Norfolk Ridge, a continental sliver located ~200-400 km southwest of active subduction at the  
168 New Hebrides trench and comprising part of the largely submerged Zealandia microcontinent  
169 (Figure 2a) (Crawford et al., 2003; Dubois et al., 1974; Lafoy et al., 2005; Mortimer et al., 2017).

170 New Caledonia exposes Late Carboniferous to Early Cretaceous basement rocks deriving  
171 from the last accretionary stages of the active southern Gondwana margin (Figure 2b,

172 ‘undifferentiated “basement” terranes’) (Aitchison & Meffre, 1992; Campbell et al., 1985;  
173 Maurizot et al., 2020b); unless otherwise noted, we adopt the naming conventions of Maurizot et  
174 al. (2020c) for New Caledonian rock units. In the Late Cretaceous, regional tectonic stresses  
175 shifted, prompting divergence and rifting associated with the breakup of the Gondwanan  
176 supercontinent. In the SW Pacific, the Tasman Sea and additional small ocean basins opened,  
177 rifting ribbons of continental crust away from the eastern margin of Gondwana (Figure 2a) (e.g.,  
178 the submarine Dampier Ridge and Lord Howe Rise, for instance; e.g., Bache et al., 2014; Davies  
179 & Smith, 1971; Mortimer et al., 2018).

180 Plate convergence in the SW Pacific began in the Late Paleocene, with an intra-oceanic  
181 NE-dipping subduction zone initiating at ~56 Ma, as recorded by the recrystallization age of  
182 high-temperature amphibolite in the basal sole of the ophiolite, and further corroborated by  
183 boninite and adakite series dikes that range from 55-50 Ma (Cluzel et al., 2006, 2012). Two  
184 distinct packages of differing protolith types and P-T-t paths are recognized to have been  
185 subducted and exhumed. The Pouébo Terrane (Figure 2c, d), which subducted first, consists of  
186 fragments of oceanic lithosphere, and was followed by the Diahot-Panié Complex (Figure 2c, d),  
187 which consists dominantly of metasediments and metavolcanic rocks (Cluzel et al., 1994; Clarke  
188 et al., 1997; Maurizot et al., 2020b). The Pouébo Terrane reached peak eclogite facies  
189 metamorphic conditions of ~2.2-2.4 GPa and ~550-600°C, equating to ~70-80 km burial depth,  
190 by ~44 Myr (Pirard & Spandler, 2017; Spandler et al., 2005; Vitale-Brovarone et al., 2013). The  
191 Diahot-Panié Complex ranges in grade from lawsonite-blueschist facies (~0.5 GPa, ~250°C) to  
192 eclogite facies (~1.8-2.2 GPa, ~500-550°C) and likely reached peak conditions at ~38 Ma  
193 (Cluzel et al., 2010; Pirard and Spandler, 2017; Potel et al., 2006; Vitale-Brovarone et al., 2018).  
194 Exhumation is interpreted to have occurred in two stages: the first stage brought the Pouébo  
195 Terrane rocks up to ~40-50 km, where they were juxtaposed with the Diahot-Panié Complex. In  
196 the second stage, the two terranes exhumed together between 38-36 Myr, with the last gasps of  
197 rapid exhumation taking place at ~34 Ma (Baldwin et al., 2007; Vitale-Brovarone et al., 2018).  
198 The arrival and partial subduction of the buoyant continental-affinity Diahot-Panié Complex  
199 effectively halted subduction and triggered the obduction of a large fragment of overlying fore-  
200 arc mantle and oceanic crust from the modern-day Loyalty Basin onto Grande Terre (referred to  
201 as the Peridotite Nappe and Poya Terrane, respectively; Brothers, 1974; Coleman, 1967).

202           2.1 Ultramafic rocks in New Caledonia

203           Ultramafic rocks occur in several discrete tectonic terranes on the island. We briefly  
204 summarize the state of knowledge with respect to the provenance of these mantle rocks,  
205 organized into tectonic groups.

206           2.1.1. The Peridotite Nappe: Massif du Sud and isolated ophiolitic klippen

207           The southern end of New Caledonia is dominated by the Massif du Sud, one of the  
208 largest coherent exposures of mantle in the world (Figure 2b). This body is notably free of  
209 significant tectonic overprint and remains attached to non-obducted lithospheric mantle in some  
210 areas (Collot et al., 1987; Patriat et al., 2018; Prinzhofer & Nicolas, 1980). Additional remnants  
211 of the large overthrust ophiolite dot the west coast of the island as small klippen. Most of the  
212 mantle portion of the Nappe consists of harzburgite and dunite, with lherzolite being found in the  
213 north (Belep, Poum, and Tiébaghi massifs; Moutte, 1982; Prinzhofer, 1981; Sécher, 1981; Ulrich  
214 et al., 2010). The transition to the crustal sequence (pyroxenite, wehrlite, and gabbro) is  
215 preserved on the southern portion of the island; the ophiolite lacks an uppermost dike complex  
216 and pillow basalts (Maurizot et al., 2020c). The ophiolite is highly geochemically depleted  
217 (Marchesi et al., 2009; Prinzhofer & Allègre, 1985), implying high degrees of melt production,  
218 and this has made this body, and in particular, the continuous exposures in the Massif du Sud, a  
219 globally-important site for studying melt transfer within the mantle and into the lower crust  
220 (Marchesi et al., 2009; Pirard et al., 2013; Pirard & Hermann, 2015; Ulrich et al., 2010).

221           2.1.2. “Basement” ultramafic bodies of Gondwanan affinity

222           Serpentinites are reported in several Gondwanan basement terranes on the island.  
223 Portions of these units experienced local low-grade (greenschist and/or lawsonite blueschist  
224 facies) overprinting by Eocene HP/LT metamorphism. In some cases, serpentinites occur  
225 amongst swaths of schist and contain tectonically-entrained oceanic crustal components (e.g.,  
226 metamorphosed pyroxenite, gabbro, basalt, chert). This ultramafic material is proposed to derive  
227 from an incoming oceanic plate that reached maximum depths of ~30-35 km beneath the  
228 overriding Gondwanan plate (‘Boghen Terrane’; Black, 1993; Cluzel & Meffre, 2002; Guérangé  
229 et al., 1977; Maurizot et al., 2020b). In other localities within the basement, serpentinites appear  
230 at faulted boundaries between coherent volcanic and abyssal sedimentary units (e.g., chert,

231 siltstones) (Maurizot et al., 2020b; Meffre et al., 1996). Published geochemical data on these  
232 rocks are lacking and a protolith origin for these serpentinites is not known.

### 233 2.1.3. Foreland accretionary units

234 Ultramafic rocks are reported to cross-cut the Montagnes Blanches Nappe, a remnant  
235 foreland fold-thrust belt preserved immediately west of the HP/LT complex (Koumac Terrane of  
236 Cluzel et al., 1994). Early interpretations link these rocks to the underlying oceanic lithosphere  
237 of the folded abyssal Montagnes Blanche Nappe sedimentary units (Brothers, 1974; Maurizot et  
238 al., 1989). These rocks have alternatively been interpreted as overthrust remnants of the  
239 Peridotite Nappe (Cluzel et al., 1995; Gautier et al., 2016; Maurizot, 2011), though a recent  
240 systematic field description of serpentinite occurrences in these units by Cluzel (2021) has  
241 pointed out inconsistencies with this hypothesis, instead positing that they are part of the upper  
242 plate. We emphasize that these hypotheses are based on field context, and published geochemical  
243 studies of the serpentinites are lacking.

### 244 2.1.4. Ultramafic and hybrid “blackwall” rocks of the HP/LT complex

245 Serpentinites occur throughout the HP/LT metamorphic belt in the NE portion of the  
246 island (Figure 2b-d). The exposed subduction complex is sprawling, spanning ~ 200 km long and  
247 ~20 km wide. The far northern area of the complex is most often referred to as the Pam  
248 Peninsula and exposes some of the best-preserved blueschists and eclogites in the complex  
249 (Figure 2c). Though observations and descriptions of serpentinite outcrops exist (e.g., Black &  
250 Brothers, 1977; Brothers & Blake, 1973; Cluzel, 2021; Lillie, 1975; Maurizot et al., 1989),  
251 geochemical and textural studies of these ultramafic rocks are sparse (Fitzherbert et al., 2004;  
252 Spandler et al., 2008), and the tectonic origin of this ultramafic material is debated. Spandler et  
253 al. (2008) interpret a seafloor origin based on major and trace element geochemistry, stable  
254 isotope measurements, and calculated temperatures of serpentinization for four serpentinite  
255 samples in the far NE portion of the complex (Figure 2c). In contrast, Fitzherbert et al. (2004)  
256 note the similarity of P-T paths and the existence of serpentinites across mapped terrane  
257 boundaries (the Diahot Terrane and Pouébo Terrane of Cluzel et al. (1995) and Fitzherbert et al.  
258 (2003)), interpreting this distribution as inconsistent with a downgoing slab origin, and instead  
259 indicating interaction with the overlying mantle. This idea can be traced to earlier interpretations  
260 that the ultramafic rocks exposed in the metamorphic complex today were part of a larger, now

261 extensively eroded overthrust “serpentinite sheet” that was incorporated from the hangingwall,  
262 based on their consistent existence at the structurally highest levels of the complex (Rawling &  
263 Lister, 2002). At a small, weathered massif outcropping in the SE portion of the complex, near  
264 the town of Yambé (Figure 2d), Fitzherbert et al. (2004) interpret the ultramafic rocks to derive  
265 from hangingwall mantle that was incorporated with the downgoing plate, subducting with it to  
266 P-T conditions past the stability of antigorite. Critically, a geochemical link between the  
267 serpentinites in the HP/LT complex and the interpretation of an overriding plate or supra-  
268 subduction mantle origin is lacking.

### 269 **3 Sample Localities and Description**

270 Twenty-three serpentinites, one chlorite schist, and one talc schist were collected in the  
271 HP/LT complex for the purposes of discerning their tectonic origin and fluid histories (Table S1;  
272 Figure 2c, d). For comparison, four serpentinites were collected from outside the HP/LT  
273 complex: two from the Boghen Terrane basement unit, one from the serpentinite sole at the base  
274 of the Peridotite Nappe, and one from Kalaa-Gomen, a small klippe of the ophiolite on the  
275 northwest coast (Figure 2b). Representative thin section photomicrographs are presented in  
276 Figures S1-S4.

#### 277 3.1 Field Context

278 Serpentinites in the northernmost portion of the HP/LT complex - defined here as an area  
279 encompassed by the Pam Peninsula and extending south along the eastern coastal road (RPN7) to  
280 the town of Balade - outcrop both as highly sheared and deformed lenses and as weathered  
281 boulders on hillslopes (Figure 2c). In highly sheared areas, the serpentinites act as a matrix for  
282 rounded pods of metamorphosed mafic, sedimentary, and other ultramafic rocks. With the  
283 exception of a small quarry south of Col d’Amos (NC19-14) and a locality in the foothills north  
284 of Ouégoa (NC18-26), all samples group spatially within the “Pouébo-Tiarì” unit of Vitale-  
285 Brovarone et al. (2018). These samples are entirely encompassed within the “mélange  
286 ophiolitique glaucophanite” unit of Maurizot et al. (1989) and fall variably within the “Pouébo  
287 metabasite dominates” and “Diahot metabasite dominates” units of Fitzherbert et al. (2004).

288 Nine samples in the HP/LT complex are located SE of the northern domain samples. A  
289 small (~ 0.5 km<sup>2</sup>) ultramafic body crops out within blueschist and eclogite facies metamafic

290 rocks near the town of Yambé (Figure 2d). Prior studies reference this ultramafic body as  
291 “Yambé” or “Yambé massif” (Fitzherbert et al., 2004; Spandler et al., 2008) and “Pwa Radèn”  
292 (e.g., Cluzel, 2021). With permission from Kanak tribal leadership, we adopt the local name  
293 given to this ultramafic body, “Poadja.” In some areas of the Poadja Massif, relict magmatic  
294 foliation is discernable at outcrop scale. Further south along the coast, two minor serpentinite  
295 outcrops (within 1 km of each other) are exposed in shear zones in beach outcrops, juxtaposed  
296 with meta-mafic blocks.

### 297 3.2 Petrographic Context

298 Serpentinites in the NE region are characterized by a dominant mineral assemblage of  
299 antigorite + talc + magnetite (Table S1; Figures 3a, b and S1) and are > 90% serpentinized, with  
300 rare relict chromian spinel (NC19-54), olivine (NC18-26B), and clinopyroxene (NC19-54).  
301 Antigorite most commonly occurs as the dominant matrix phase, forming interlocking crystals  
302 with variably preserved evidence for mesh texture. Some samples exhibit anhedral fine-grained  
303 (<10  $\mu\text{m}$ ), recrystallized antigorite intergrown with talc and less commonly, tremolite (e.g.,  
304 NC18-15C, NC18-15D, NC18-22A). In some cases, well-developed bastite pseudomorph  
305 textures are evidenced by clumped aggregates of coarser-grained (~100-200  $\mu\text{m}$ ) euhedral  
306 antigorite crystals accompanied by euhedral magnetite (~10’s of  $\mu\text{m}$ ) (e.g., NC19-86). Magnetite  
307 additionally occurs as a matrix phase as single subhedral grains (~10’s of  $\mu\text{m}$  up to ~1 mm) or as  
308 polymineralic aggregates of smaller euhedral grains (~10’s of  $\mu\text{m}$ ). In deformed samples these  
309 aggregates lie within the foliation (e.g., NC19-54, NC18-22A). In rare cases, relict chromite is  
310 preserved in the core of grains mantled by ferritchromite and rimmed by magnetite (Figure 3a).  
311 Two types of veins assemblages are present as cross-cutting networks: antigorite-magnetite  
312 (NC19-86; Figures S1e, j) and antigorite-tremolite (NC19-94; Figure 3b).

313 Serpentinites in the SE region are characterized by the presence of relict phases  
314 (orthopyroxene and olivine) and range between ~50 to ~90% serpentinized (Table S1; Figures  
315 3c-f and S2). Samples from this locality notably lack talc (with the exception of NC19-158), and  
316 four samples contain the Fe-Ni alloy awaruite as an accessory phase (Figure 3d). Oxide textures  
317 show varying degrees of retrogression from skeletal chromite with magnetite rims (Figure 3c) to  
318 chromian magnetite cores complexly replaced by magnetite (Figure 3e). Texturally-late brucite

319 veins are observed in one sample (NC18-39A). Mesh textures are less developed compared to  
320 the complete pseudomorphing observed in the NE (Figure 3f).

## 321 **4 Methods**

### 322 4.1 Whole-rock major and trace element geochemistry (XRF, ICP-MS)

323 Twenty-three serpentinites, one talc schist, and one chlorite schist were analyzed for  
324 whole-rock major and trace element compositions. Major element analyses were acquired by  
325 lithium tetraborate fusion X-ray fluorescence methods at the GeoAnalytical Laboratory  
326 (Washington State University, USA; WSU) and Franklin & Marshall College (Pennsylvania,  
327 USA; F&M). Hand-picked fresh chips of each sample were powdered and fused on-site.  
328 Additional details on preparation and fusion are reported in supporting information S1. At WSU,  
329 major elements were analyzed on a ThermoARL Advant'XP+sequential X-ray fluorescence  
330 (XRF) spectrometer using the preparation and analytical procedure described in detail by  
331 Johnson et al. (1999) and Kelly (2018). At F&M, major elements were analyzed on a Malvern  
332 PANalytical Zetium X-ray fluorescence spectrometer. Trace element concentrations were  
333 acquired at WSU and the University of Rhode Island (USA). Digestions and dilution were  
334 performed on-site. At WSU, trace elements were analyzed on an Agilent quadrupole ICP-MS  
335 using the method of Knaack et al. (1994). Analytical precision is <5% for REE's and <10% for  
336 the remaining elements. At University of Rhode Island, trace elements were analyzed on a  
337 Thermo X-Series 2 quadrupole ICP-MS following the method of Savov et al. (2005).  
338 Interference corrections were applied for TiO on Zn, Ba<sup>++</sup> on Ga, and CrO on Nb. Analytical  
339 precision is <5% for most elements, and precision for Cr and Ni was <2%. Two samples (NC18-  
340 15D, NC18-49) were analyzed by all three labs (Table S2, S3).

### 341 4.2 Oxygen and hydrogen stable isotope geochemistry

342 Oxygen and hydrogen isotope compositions of serpentine, talc, and magnetite mineral  
343 separates were measured at the University of Texas at Austin using a ThermoElectron MAT 253  
344 mass spectrometer. Serpentine samples were coarsely crushed and handpicked under a  
345 binocular microscope to ensure purity of mineral separates. Handpicked serpentine and talc  
346 grains were washed with dilute HCl to remove any trace carbonate material. Approximately 2.0  
347 mg of each mineral separate were analyzed using the laser fluorination method of Sharp (1990)

348 in which samples were heated by a CO<sub>2</sub> laser in the presence of a BrF<sub>5</sub> atmosphere to liberate  
349 oxygen. Liberated oxygen was cryogenically purified and analyzed as O<sub>2</sub>. Precision and accuracy  
350 of oxygen analyses were verified through garnet standard UWG-2 ( $\delta^{18}\text{O} = +5.8\%$ ) (Valley et al.,  
351 1995), in-house olivine standard San Carlos ( $\delta^{18}\text{O} = +5.2\%$ ), and in-house quartz standard  
352 Lausanne-1 ( $\delta^{18}\text{O} = +18.1\%$ ). All  $\delta^{18}\text{O}$  values are reported relative to SMOW, where the  $\delta^{18}\text{O}$   
353 value of NBS-28 is +9.7‰. The error on each  $\delta^{18}\text{O}$  analysis is  $\pm 0.1\%$ , based on the long-term  
354 average of standard analyses. Seven samples were run in duplicate to ensure reproducibility and  
355 consistency over four analytical runs.

356 Hydrogen isotope ratios were measured using the method of Sharp et al. (2001). Samples  
357 were hand-powdered using an agate mortar and pestle. Approximately 1 mg of each sample were  
358 loaded into silver foil capsules, dried under vacuum at 70° C for 24 h, transferred to a Costech  
359 zero-blank autosampler, and flushed with He gas. Samples were measured by continuous-flow  
360 mass spectrometry using a ThermoElectron TC/EA (high-temperature conversion elemental  
361 analyzer) coupled to the ThermoElectron MAT 253 mass spectrometer. Four internationally  
362 referenced and certified standard materials (IAEA-CH7, NBS-22, USGS-57, USGS-58) and one  
363 in-house working glass standard were analyzed with the samples throughout the run. Raw  $\delta\text{D}$   
364 values were corrected for instrumental drift and normalized to SMOW using a calibration curve  
365 generated from the measurements of the standard reference materials. Error based on the  
366 reproducibility of standards measured in the analytical runs is  $\pm 2\%$ .  $\delta\text{D}$  values referenced in the  
367 text and plotted are the mean of two individual replicate analyses.

#### 368 4.3 Raman spectroscopy

369 Raman spectra were acquired on eight serpentinite samples (two samples from Group I,  
370 four samples from Group II, one from the Bogen Terrane, and the sample from Kalaa-Gomen).  
371 In situ spot analyses on 30  $\mu\text{m}$  polished thin sections were acquired on a Witec Alpha 300R  
372 confocal Raman microscope at the Characterization Facility, University of Minnesota. The  
373 confocal Raman microscope is equipped with a UHTS300 spectrometer and DV401 CCD  
374 detector. Spectra were acquired with a frequency doubled Nd:YAG 532 nm laser, a 1,800 g/mm  
375 grating, and a 100x objective. Spot size was  $\sim 1 \mu\text{m}$  in diameter. Each spectra resulted from the  
376 average of two 20 s acquisitions to optimize the signal/noise ratio. Two spectral intervals were  
377 measured: a low-wavenumber region (100-1200  $\text{cm}^{-1}$ ) for structural bonding characterization and

378 a high-wavenumber region (3300- 4050  $\text{cm}^{-1}$ ) for characterization of hydroxyl groups. A range  
379 of relevant textural settings were targeted in each thin section (e.g., serpentine matrix, veins, and  
380 pseudomorphs). Data were processed using the WITec Project Five+ software. Raw spectra  
381 underwent background subtraction followed by smoothing using a third-order polynomial  
382 Savitzsky-Golay filter. Serpentine species were identified by comparison to previously published  
383 data (Auzende et al., 2004; Groppo et al., 2006, Petriglieri et al., 2015; Tarling et al. 2018).

## 384 **5 Results**

### 385 5.1 Whole rock major elements

386 Serpentinites from the HP/LT complex display differences in  $\text{SiO}_2$ ,  $\text{Al}_2\text{O}_3$ ,  $\text{MgO}$ , and  
387  $\text{CaO}$  contents and cluster in two distinct geochemical groupings (Table 1; Figure 4). One group  
388 of serpentinites ( $n = 15$ ; herein referred to as Group I) is depleted in  $\text{MgO}$  compared to other  
389 serpentinites (herein referred to as Group II,  $n = 9$ ):  $34.05 \pm 3.34$  wt% in Group I versus  $40.19 \pm$   
390  $3.20$  wt% in Group II. Group I serpentinites contain higher  $\text{Al}_2\text{O}_3$  contents than Group II ( $2.34 \pm$   
391  $1.47$  versus  $0.75 \pm 0.34$  average wt%, respectively). Group I samples are generally elevated in  
392  $\text{SiO}_2$  compared to Group II, though they overlap within uncertainty, with averages of  $44.96 \pm$   
393  $5.23$  wt% and  $41.13 \pm 2.13$  wt%, respectively.  $\text{Fe}_2\text{O}_{3(\text{T})}$  contents do not vary significantly  
394 between the two groups, though samples in Group I display a broader range of variation ( $7.92 \pm$   
395  $1.85$  wt % versus  $7.38 \pm 0.68$  wt% for Group II).  $\text{CaO}$  concentrations in the HP/LT serpentinites  
396 overall are  $<0.5$  wt%, with the exception of the three least serpentinized samples (Table 1 and  
397 Figure S2); all Group II samples located in the SE portion of the complex (0.53, 0.57, and 1.08  
398 wt%). The ophiolitic reference sample from Kalaa-Gomen (NC19-178) has 0.66 wt%  $\text{CaO}$ .  
399 Samples have a range of loss-on-ignition (LOI) values, from 5.25 to 12.64%, indicating varying  
400 degrees of hydration, with an overall average of  $10.43\% \pm 2.77\%$ .  $\text{Na}_2\text{O}$ ,  $\text{K}_2\text{O}$ , and  $\text{P}_2\text{O}_5$  are  
401 close to or below detection limits.

402 The chlorite schist (NC19-85) is elevated with respect to the talc schist (NC19-169) in  
403  $\text{Al}_2\text{O}_3$ ,  $\text{Fe}_2\text{O}_{3(\text{T})}$ , and  $\text{TiO}_2$ , whereas the talc schist is elevated in  $\text{SiO}_2$  and  $\text{MgO}$  (Table 1). The  
404 chlorite schist (NC19-85) has  $\text{CaO}$  and  $\text{P}_2\text{O}_5$  contents of 2.47 and 1.88 wt%, respectively, due to  
405 the presence of  $\sim 5\%$  modal abundance apatite.

## 406 5.2 Whole-rock trace elements

407 Group I and II samples are overall depleted in trace elements with respect to primitive  
408 mantle (Figure 5a, b). Both groups show enrichments in Cs and Pb and negative Rb and Nb  
409 anomalies. Group I samples show marked Th and U enrichments and a strong negative Sr  
410 anomaly compared to Group II. Group I samples show greater overall enrichment in  
411 middle to heavy rare-earth elements (M-HREE; Sm, Eu, Gd, Tb, Dy, Y, Ho, Er, Yb, Lu)  
412 compared to Group II (Figure 5c-f). Differences in the pattern of light-rare earth elements  
413 (LREE; La, Ce, Pr, Nd, Pm) to HREE most clearly distinguish the two groups ( $\text{La}_N/\text{Ho}_N = 1.66 \pm$   
414  $1.33$  for Group I and  $6.59 \pm 1.92$  for Group II; normalized to primitive mantle).

415 The chlorite schist (NC19-85) and talc schist (NC19-169) samples display distinct  
416 enrichments in trace elements. The chlorite schist is enriched in Li, Sc, V, Cu, Zn, Sr, Y, Zr, Nb,  
417 Ba, La, Ce, Pr, Nd, Sm, Eu, Tb, Gd, and Dy relative to the talc schist. Conversely, the talc schist  
418 is enriched in Cr and Ni relative to the chlorite schist.

## 419 5.3 Stable isotope geochemistry

## 420 5.3.1 Oxygen isotopes

421 Serpentine from the high-pressure complex displays a wide range of oxygen isotope  
422 values: from +5.1 to +10.2‰ (Table 2 and Figure 6a, b). Group I samples are between +6.7 and  
423 +10.2‰, whereas Group II samples are between +5.1 to +8.0‰. The mean serpentine  $\delta^{18}\text{O}$  value  
424 for Group I is  $+8.7 \pm 0.9\text{‰}$  ( $n = 15$ ) and  $+5.5 \pm 0.4\text{‰}$  ( $n = 9$ ) for Group II. A Group II sample  
425 (NC18-39A) shows a 1‰ increase in  $\delta^{18}\text{O}$  between serpentine extracted from the sample interior  
426 (+5.4‰) and serpentine from an outer altered rind (+6.4‰).  $\delta^{18}\text{O}$  sample replicates reproduced  
427 within 0.2‰, with the exception of two samples, NC18-15D and NC18-22A, which show  
428 variability of 1.8‰ and 0.9‰, respectively. Comparative samples from the Boghen Terrane,  
429 Kalaa-Gomen Massif, and the Peridotite Nappe serpentinite sole have  $\delta^{18}\text{O}$  values of +7.5‰  
430 (average of two samples), +5.7‰, and +6.5‰, respectively.

431 Oxygen isotopes in magnetite were measured in three samples from the NE part of the  
432 complex: a serpentinite (NC19-86), a chlorite schist (NC19-85), and a talc schist (NC19-169).  
433 The  $\delta^{18}\text{O}$  value of magnetite is +1.5‰ in the serpentinite and +2.4‰ in the chlorite schist. In the  
434 talc schist, two separate grain size fractions were measured, 125-250  $\mu\text{m}$  and  $>710 \mu\text{m}$ . The 125-

435 250  $\mu\text{m}$  grain size fraction has a  $\delta^{18}\text{O}$  value of +4.3‰, whereas the >710  $\mu\text{m}$  has a value of +4.6  
436  $\mu\text{m}$ . Oxygen isotopes in talc from two samples (one from the SE and one from the NE), were  
437 +9.0 and +10.5‰, respectively.

### 438 5.3.2. Hydrogen isotopes

439  $\delta\text{D}$  values of serpentine in the high-pressure complex range from -79 to -29‰ (Figure  
440 6a). Group I sample range between -76 and -29‰ and Group II samples range between -79 and -  
441 39‰. The mean serpentine  $\delta\text{D}$  value is  $-44 \pm 10\text{‰}$  ( $n = 30$ ) for Group I and  $-52 \pm 14\text{‰}$  ( $n = 18$ )  
442 for Group II. The relatively large standard deviation in both groups derives from three samples  
443 (one in Group I and two in Group II) that have  $\delta\text{D}$  values between -79 and -70‰. Without these  
444 values, the remaining samples from Group I exhibit a more restricted range of  $\delta\text{D}$  values from -  
445 49 to -32, with an average of  $-41 \pm 5\text{‰}$  ( $n = 28$ ). Group II ranges from -59 to -39‰, with an  
446 average of  $-46 \pm 8\text{‰}$  ( $n = 14$ ). Comparative samples from the Boghen Terrane, Kalaa-Gomen  
447 Massif, and the Peridotite Nappe serpentinite sole have  $\delta\text{D}$  values of -81‰ (average of two  
448 samples), -85‰, and -82‰, respectively. Across all samples,  $\delta\text{D}$  sample replicates reproduced  
449 within 2‰, on average.

### 450 5.4 Raman spectroscopy

451 Serpentine has three primary structural polymorphs that vary over  $P$ - $T$  space: the low- $T$   
452 form is chrysotile, followed by lizardite and antigorite. Diagnosing the polymorph in exhumed  
453 serpentinites can aid in retrieving information about its prograde and/or retrograde path and  
454 alteration. Serpentine in two samples from Group I and four samples from Group II was found to  
455 be antigorite (only) in contrast to lizardite identified in comparative samples from the Boghen  
456 Terrane basement unit and Kalaa-Gomen massif in the Peridotite Nappe (Figure 7 and S5-6).

### 457 5.5 Categorization of New Caledonia HP/LT serpentinites

458 As presented above, serpentinites in the high-pressure metamorphic complex cluster in  
459 two distinct groups, revealed by petrography, major and trace element, and stable isotope  
460 geochemistry. The significance of these groups and their composition will be discussed in the  
461 next section. The results are summarized as follows:

462 Group I: >90% serpentinized, common assemblage of antigorite + talc + magnetite,  
463 lower, more homogeneous MgO contents (relative to Group II),  $\delta^{18}\text{O}$  values between  
464 +6.7‰ and 10.2‰, flat M-HREE patterns;

465 Group II: ~50-90% serpentinized, notable preservation of orthopyroxene and olivine and  
466 distinct presence of awaruite, higher MgO contents (relative to Group I),  $\delta^{18}\text{O}$  between  
467 +5.1‰ and +8.0‰, distinct curved LREE to HREE pattern compared to Group I.

## 468 **6 Discussion**

469 Prior studies of serpentinites in the HP/LT terrane of New Caledonia have disagreed on  
470 the tectonic origin of the mantle protolith (Fitzherbert et al., 2004; Spandler et al., 2008). Our  
471 results indicate the existence of two geochemically-distinct groups of serpentinites in the  
472 blueschist- to eclogite-facies portions of the complex. This heterogeneity may derive from (1)  
473 geochemical differences in the original mantle source material, (2) processes occurring  
474 throughout serpentinization, (3) subsequent metamorphism during subduction and exhumation,  
475 or (4) a combination of the above.

### 476 6.1 Assessing major and trace element mobility

477 The major and trace element compositions of exhumed serpentinites result from (a) the  
478 original composition and melt history of the parent peridotite, (b) fluid-rock reactions occurring  
479 at the source location for serpentinization (e.g., seafloor, mantle wedge), and (c) fluid-rock  
480 reactions occurring during subduction and exhumation. Extensive study of variably serpentinized  
481 abyssal and mantle wedge peridotites and serpentinites in exhumed subduction complexes has  
482 demonstrated high-field strength elements (HFSE; Nb, Ta, Zr, Hf) and REE are generally (but  
483 not wholly) immobile during serpentinization and aqueous fluid alteration and can be used to  
484 discern information about protolith composition and pre-serpentinization magmatic processes  
485 (e.g., Deschamps et al., 2013; Kodolányi et al., 2012; Niu, 2004; Parkinson & Pearce, 1998;  
486 Savov et al., 2005; Scambelluri et al., 2004). By contrast, major elements and FME (e.g., Li, Pb,  
487 U, Cs, Sr, Ba) must be interpreted with additional caution, as serpentinization is not isochemical  
488 with respect to some of these elements and/or they are more readily mobilized during fluid  
489 interaction over the course of subduction and exhumation (e.g., Cannao et al., 2016; Malvoisin,  
490 2015; Peters et al., 2017). With this in mind, we first assess the degree to which major and trace

491 elements in the New Caledonia HP/LT serpentinites may have been mobilized, or whether they  
492 otherwise retain faithful geochemical signatures of their initial mantle protolith.

493 Ratios of immobile trace elements (e.g., LREE, HFSE vs HREE; La/Yb, Zr/Yb, Hf/Yb,  
494 Nd/Yb) are observed to vary independently of LOI for both groups of HP/LT serpentinites  
495 (Figure 8). This result, combined with the observed similarity of intra-group REE patterns for  
496 Groups I and II (Figure 5), provides initial confidence in the retention of protolith mantle  
497 geochemical signatures for these elements (c.f. Savov et al., 2005). For further assessment, plots  
498 of LREE (La, Ce, Pr, Nd) versus HFSE (Nb, Ta, Zr, Hf) elucidate whether a common process or  
499 processes were responsible for the enrichment or depletion of these groups of elements (c.f. Niu,  
500 2004). It is worth noting that LREE are more readily mobilized by aqueous fluids than MREE  
501 and HREE, so this test is a conservative indicator of trace element and REE immobility.

502 Group I LREE's are almost entirely decoupled from HFSE (Figure 9). Indications of a  
503 once-coupled relationship between the LREE and HFSE are partially retained in a few samples,  
504 as indicated by consistent low abundances that correlate somewhat more linearly (but to a degree  
505 no longer statistically significant). More often, however, these samples have been overprinted by  
506 a process or processes that added LREE (Figure 9). In contrast, statistically significant  
507 correlations are observed for Group II serpentinites between the LREE and Zr and Nb ( $R_{\text{LREE-Zr}}$   
508  $_{(\text{avg})} = 0.942 \pm 0.027$ ,  $R_{\text{LREE-Nb}}_{(\text{avg})} = 0.678 \pm 0.024$ ) (Figure 9). Notably, LREE appear decoupled  
509 from Ta and Hf ( $R_{\text{LREE-Ta}}_{(\text{avg})} = -0.267 \pm 0.037$ ,  $R_{\text{LREE-Hf}}_{(\text{avg})} = 0.308 \pm 0.106$ ). Of the HFSE, Zr  
510 and Nb (here coupled with LREE) are lighter in mass than Ta and Hf. Niu (2004) addresses the  
511 potential importance of mass-dependent effects on the observed magmatic fractionation of Nb/Ta  
512 and Zr/Hf ratios in global abyssal peridotite datasets, proposing that elevated LREE abundances  
513 could be produced or enhanced by mass-dependent transfer rates, but notes that observational  
514 tests of this hypothesis are necessary. These data possibly corroborate this hypothesis,  
515 particularly given that none of the four elements correlate with LOI. However, the possibility  
516 that this decoupling reflect later aqueous alteration processes cannot be ruled out, though it is  
517 unclear whether subduction zone temperatures would be sufficiently high enough to mobilize  
518 these HFSE.

519 In summary, both groups show variations in trace and REE independent of LOI - a  
520 valuable first indicator for retained magmatic trace element signatures. Strong correlation

521 between LREE and HFSE in Group II samples bolsters this argument. Observed mobility in  
522 Group I LREE does not preclude us from utilizing the REE data to ascertain a tectonic setting for  
523 the mantle protolith, as there is no demonstrated correlation between the M-HREE with LOI;  
524 though care must be taken in interpreting the significance of LREE abundances and their  
525 contribution to the overall shape of L-HREE trends.

## 526 6.2 Serpentinization processes and fluid interactions

527 Within the ultramafic rock system, oxygen and hydrogen isotopes have been widely  
528 utilized to discern the source of serpentinizing fluids and subsequent post-serpentinization fluid  
529 histories (e.g., Alt and Shanks, 2006; Burkhard and O'Neil, 1988; Früh-Green et al., 1990, 2001;  
530 Kyser et al., 1999). Ultimately, stable isotope values are the amalgamated product of several  
531 important variables – the stable isotope composition of the interacting fluid, the fluid-rock ratio,  
532 the composition of the reactive solid phase(s) in the system, and the fractionation factors  
533 between these components and the fluid. Stable isotope data for the HP/LT serpentinites indicate  
534 differing serpentinizing fluid compositions and/or  $T$  conditions for serpentinization between the  
535 two groups of samples. Group II  $\delta^{18}\text{O}$  values ( $+5.5 \pm 0.4\text{‰}$ ) cluster tightly around the typical  
536 upper mantle value ( $+5.4\text{‰}$ ), indicating little to no additional alteration of the primary mantle  
537 signature during serpentinization, subduction, or exhumation (Figure 6). This assessment is  
538 supported by recent stable isotope modeling of the ophiolite that indicates limited interaction of  
539 slab sediment-derived fluids within New Caledonia's mantle wedge during the initial phases of  
540 subduction (Ulrich et al., 2020). Moreover, these authors discern, on the basis of Sr isotopes and  
541 low abundances of sediment-derived elements such as As and Sb (Deschamps et al., 2013), that  
542 the input of subducted sediments was low at the time of serpentinization of the mantle wedge,  
543 and instead the dehydration of altered oceanic crust comprised the dominant fluid source.  
544 Though our data do not include measurements of As and Sb, we observe similarly low degrees of  
545 elements typically regarded as classic markers of serpentinization in the mantle wedge via  
546 shallow dewatering fluids released from slab sediments and lower- $T$  metamorphic dehydration  
547 reactions (e.g., Cs, Sr, Rb, Li) (Figure 1). The narrow range of  $\delta^{18}\text{O}$  values across all degrees of  
548 hydration (as indicated by LOI %) supports a consistent temperature of serpentinization and/or a  
549 consistent fluid composition (Figure 6). The close relation between the  $\delta^{18}\text{O}$  values of Group II

550 serpentinites and antigorite within slab-derived tremolite-antigorite veins in the Peridotite Nappe  
551 also supports a similar source for serpentinizing fluids.

552 By contrast, Group I samples show increased and variable  $\delta^{18}\text{O}$ , which may be  
553 interpreted to reflect: (1) interaction with metamorphic fluids with a sedimentary component, (2)  
554 differing temperatures of serpentinization in a seafloor environment, or (3) a mix of these two  
555 influences. Both end-member explanations are plausible - all but two Group I samples are  
556 located within 2 km of interpreted boundaries between the Pouébo Terrane and the sediment-  
557 dominated Diahot-Panié Complex. Moreover, significant fluid fluxing is evident for these  
558 samples given major element concentrations, which show a clear deviation from the terrestrial  
559 array as a function of increasing modal abundances of talc (Figure 6). The development of talc-  
560 rich serpentinite and hybrid rock assemblages in the NE portion of this HP/LT complex has been  
561 attributed to high fluid flux-driven metasomatism at depth and is the source of a separate study  
562 by Spandler et al. (2008).

563 A suite of discriminant fluid-mobile trace element diagrams complements our  
564 interpretation of significantly different fluid and tectonic histories for Groups I and II. FME's in  
565 serpentinites are an sensitive recorder of fluid interactions, in part because peridotite protoliths  
566 are depleted in these elements, so increases in their concentration are attributable to fluid  
567 interactions (e.g., Peters et al., 2017; Scambelluri et al., 2019). Recent re-analysis and refinement  
568 of compiled serpentinite data has also demonstrated that these elements are sensitive tracers of  
569 the tectonic environments of serpentinization (Peters et al., 2017). For the New Caledonia HP/LT  
570 serpentinites, plots of fluid-mobile element enrichments (e.g., Ba, Cs) relative to fluid-immobile  
571 elements such as Yb show compelling trends (Figure 10). Ba in Groups I and II (Figure 10a)  
572 indicates a mantle wedge origin for Group II samples, which are relatively enriched compared to  
573 Group I samples, which fall squarely within the field for mid-ocean ridge serpentinites. This  
574 trend is not observed for Cs, which we interpret as becoming enriched in Group I samples during  
575 intense fluid flow and deformation, and possible interaction with neighboring sediments from the  
576 Diahot-Panié Complex. Cs in Group II falls lower than compiled forearc data, commensurate  
577 with our interpretations for limited influence of sedimentary-derived fluids based on stable  
578 isotope data. This Cs depletion is apparent in a plot of Cs vs fluid-immobile Yb, though the data  
579 in this context better overlap with the range of observed values for drilled or dredged forearc  
580 samples, and the Group I samples correlate well with the compiled mid-ocean ridge dataset.

581 Trends between U and Th enrichments show that Group I samples lack the seafloor U  
582 enrichment that defines some (but not all) of the mid-ocean ridge dataset (Figure 10c).

### 583 6.3 Tectonic origin of New Caledonia HP/LT-complex serpentinites

584 Given evidence presented above, we interpret differing tectonic origins for serpentinites  
585 in the NE and SE portions of the terrane:

586 Group I: Found dominantly in the NE part of the complex, these serpentinites are  
587 remnants of lithospheric mantle from the downgoing plate (Figure 11a). They experienced  
588 progressive serpentinization on or near the ocean floor prior to subduction and then faced high-  
589 fluid-rock ratios, metasomatism leading to the development of talc-bearing assemblages, and  
590 deformation in the subduction channel. The formation of these rocks was possibly associated  
591 with the development of several major shear zones, which facilitated slicing of the complex at  
592 depth and have given parts of the Pouébo Terrane the appearance of a *mélange*. This geodynamic  
593 interpretation is supported by recent reevaluations of the architecture of the belt (Maurizot et al.,  
594 2020c; Vitale-Brovarone et al., 2018) and consistent with our observation of the proximity of  
595 serpentinites to major unit boundaries and faults (e.g., NC18-22A, NC18-26B, NC19-63) and  
596 their prevalence as matrix hosts for dismembered blocks in km-scale shear zones. It is plausible  
597 that the pre-subduction abyssal environment for the future Pouébo Terrane ultramafic rocks was  
598 characterized by lower-T conditions, consistent with stable isotope data presented here (Figure  
599 6b). Seismic imaging of the New Caledonia Basin to the west of the island has revealed thinned  
600 continental crust interpreted to consist of a significant volume of serpentinized upper mantle and  
601 resembling the structure of crust formed during slow, low-T amagmatic seafloor spreading  
602 (Klingelhoefer et al., 2007).

603 Group II: These samples cluster in the southern portion of the complex, comprising the  
604 Poadja Massif. Incorporated onto the top of the slab prior to the onshore obduction of the  
605 Peridotite Nappe, this slice of mantle wedge was subducted and exhumed intact, with striking  
606 preservation of relict minerals and comparatively minor degrees of fluid alteration, as evidenced  
607 by  $\delta^{18}\text{O}$  isotope values that remain near the pristine upper mantle average and lower degrees of  
608 LREE and FME (Cs, U, Pb, and Sr) enrichment relative to other global forearc mantle settings  
609 (Figure 11b). We interpret these data to reflect the lack of a strong sedimentary-derived fluid flux  
610 during serpentinization of these rocks in their mantle wedge setting, and this is supported by

611 independent evidence from analyses of slab-derived tremolite vein assemblages at the base of the  
612 obducted Peridotite Nappe (Cluzel et al., 2020). This muted enrichment of LREE and FME also  
613 indicates that later overprinting by meta-sedimentary derived fluids during transport within the  
614 subduction channel was limited. The samples display characteristic REE patterns that remarkably  
615 resemble the harzburgitic mantle of New Caledonia's Peridotite Nappe (Figure 11b).

#### 616 6.4 Relevance for the architecture of the New Caledonia HP/LT complex

617 In the NE portion of the complex, our combined field observations and geochemical data  
618 suggest that Group I (downgoing-slab) serpentinites: (a) overwhelmingly appear in the highest-  
619 grade portions of the complex, within the oceanic affinity Pouébo Terrane, and (b) show distinct  
620 geochemical markers for high degrees of fluid interaction and deformation during subduction  
621 and/or exhumation (i.e., elevated  $\delta^{18}\text{O}$  values, decoupled LREE's, enriched FME's such as Cs).  
622 These observations are broadly consistent with recent re-interpretations of this subduction  
623 complex by Vitale-Brovarone et al. (2018), which posits the existence of two accretionary  
624 domains preserved in a nappe-type belt formed by progressive underplating and stacking. The SE  
625 portion of the complex is far less studied: the existence of Group II mantle wedge serpentinites  
626 carries implications for the structural level of the subduction zone sampled by rocks in the  
627 immediate vicinity of the Poadja Massif. The existence of mantle wedge serpentinites adds to  
628 independent observations made by Cluzel (2021) of the presence of hangingwall mafic rocks in  
629 lower-grade portions of the Diahot-Panié Complex further north. Integrating these observations  
630 into a unified subduction complex-scale picture of preserved lithostratigraphy requires further  
631 studies. Nevertheless, these observations provide compounding evidence for greater structural  
632 coherence within the New Caledonia subduction "mélange" than has previously been posited.

#### 633 6.5 Implications for slab-mantle wedge interactions

634 Our finding of mantle wedge material within the exhumed HP/LT complex on New  
635 Caledonia provides direct evidence for interaction with the hangingwall mantle in this Eocene  
636 subduction zone. Geochemical modeling has demonstrated the importance of the mantle wedge  
637 as a reservoir for water and fluid-mobile elements that contribute to arc magma isotope and  
638 elemental budgets (e.g., Debret et al., 2019, 2020; Ribeiro & Lee, 2017; Savov et al., 2005,  
639 2007), and there are strong conceptual bases, observational evidence, and modeled predictions

640 for the incorporation and downward dragging of mantle wedge material in some subduction  
641 zones (e.g., Bebout & Barton, 2002; Bebout, 2007; Cloos & Shreve, 1988; Malatesta et al., 2012;  
642 Peacock & Hyndman, 1999; Savov et al., 2005). New Caledonia provides an important natural  
643 rock record comparison for geodynamic modeling: particularly for outcomes in which  
644 exhumation of downgoing plate mantle *and* overlying mantle wedge material is predicted (e.g.,  
645 Gerya & Stockert, 2006; Gerya et al., 2002; Malatesta et al., 2012). In these cases, the rheology  
646 of serpentine and evolving hydration state of the ultramafic material are critical to the locus of  
647 the weak, low-viscosity subduction channel and eventual migration of the plate interface  
648 upwards into the mantle wedge. The development of talc in the overlying mantle assemblage  
649 provides a possible physiochemical mechanism for this migration, and its stability in the  
650 ultramafic chemical system may even control the depth of plate decoupling (Peacock & Wang,  
651 2021).

652         This hypothesis is interesting to consider in light of our observations of relatively  
653 undeformed, nearly talc-absent mantle wedge assemblages observed in the SE and deformed,  
654 talc-bearing downgoing mantle assemblages in the NE. A local bulk assemblage-induced  
655 rheological switch in the mantle wedge and consequent avulsion of the slab-mantle interface  
656 could be broadly consistent with the results presented here. In this scenario, deformation rapidly  
657 re-localizes in the new region of weakness and a stranded slice of mantle wedge material is  
658 incorporated atop the downgoing slab. This mantle may feasibly have already experienced partial  
659 high-T serpentinization from fluxed aqueous dehydration fluids (consistent with stable isotope  
660 data presented here) and might largely escape prolonged intense deformation, because the  
661 subduction interface was localized first below, and then above the mantle wedge slice in  
662 rheologically weaker assemblages (consistent with observed petrographic textures and field  
663 observations).

664         Tectonic erosion of the mantle wedge, and the type of HP/LT ultramafic material it  
665 produces, contrasts markedly with the processes that retrieve lithospheric mantle under  
666 subducted oceanic crust. Slicing and nappe development along lithologic (rheologic)  
667 heterogeneities in the slab are commonly invoked as ways by which downgoing mantle may be  
668 incorporated into the subduction channel (e.g., Angiboust & Agard, 2010; Guillot et al., 2009;  
669 Hermann et al., 2000; Wakabayashi, 1992). During these processes, the mantle is juxtaposed and  
670 reacts with sedimentary and mafic components of the slab, as reflected by stable isotope

671 compositions and Si and trace element enrichments. The data presented here for New  
672 Caledonia's NE serpentinites reflect this type of metamorphic history, including their spatial  
673 concentration within the oceanic Pouébo Terrane and proximity to inferred boundaries with the  
674 Diahot-Panié Complex.

## 675 **7 Summary**

676 In this study, we resolve two petrographically, geochemically, and spatially distinct  
677 groups of serpentinites within New Caledonia's HP/LT subduction complex. Our work  
678 reconciles existing disparate interpretations of the tectonic origin of these rocks, with  
679 implications for slab-mantle interaction during subduction. In the NE portion of the complex  
680 serpentinite geochemistry and field relations indicate a downgoing slab origin. By contrast, the  
681 chemistry of serpentinites in the SE points to a mantle wedge origin, indicating incorporation and  
682 subduction of upper plate material. The exhumation of serpentinites from these two different  
683 geodynamic settings within a single HP/LT complex is not common in the natural rock record,  
684 but predicted for certain modeled scenarios as a function of serpentine rheology and hydration  
685 state, among other subduction parameters. The mineralogy, chemistry, and spatial distribution of  
686 New Caledonia's HP/LT serpentinites hold clues for understanding the architecture of this  
687 subduction complex, and more broadly, for the modeled dynamics of deep tectonic slicing of  
688 subducted oceanic plates and mass transfer between the upper and lower plates.

## 689 **8 Acknowledgments**

690 We thank Chief Guiart and Chief Heiec, tribal leaders of Yambé and Diahoué,  
691 respectively, for their authorization to access the Poadja Massif, and Mr. Hervé and family for  
692 their interest in our work and assistance in communicating our presence and purpose to the  
693 community. At DIMENC (New Caledonia), Pierre Maurizot and Bernard Robineau are thanked  
694 for thoughtful discussions and granting use of rock processing facilities. The UT-Austin High-  
695 Temperature Stable Isotope lab is thanked for assistance with run setup and data quality  
696 evaluation, particularly Jaime Barnes, Jeff Cullen, and Dan Brecker. We acknowledge Anette  
697 von der Handt (UMN EPMA) and Bing Luo (UMN Raman) for technical expertise and  
698 assistance. Ashley Steiner and Charles Knaack (WSU), Katie Kelley and Janine Andrys (URI),  
699 and Stan and Karen Mertzman (Franklin & Marshall College) are thanked for assistance in

700 acquiring whole rock analyses. Mario Ramos Arias (UNAM) is thanked for discussion and  
701 participation during the collection of a subset of these samples. This work was partially  
702 supported by two GSA Graduate Student Research Grants to N. Raia with additional support  
703 from NSF grant EAR-1949895 (to D.L. Whitney). Funding for the electron microprobe facility  
704 used in this research was provided by NSF grant EAR-1625422. The Characterization Facility of  
705 the College of Science and Engineering at the University of Minnesota receives partial support  
706 from NSF through the MRSEC program.

## 707 **9 Open Research**

### 708 Data Availability Statement

709 To ensure the accessibility and discoverability of the samples used in this research, and to  
710 align with the National Science Foundation's guidelines of effective data practices, all samples  
711 used in this study have been registered with IGSN Global Sample Numbers through the System  
712 for Earth Sample Registration (SESAR). SESAR is maintained by the GeoInformatics Research  
713 Group of the Lamont-Doherty Earth Observatory. <https://www.geosamples.org/> Accessed 17  
714 February 2022. Whole rock and stable isotope data presented in this paper will be submitted for  
715 archival in EarthChem data repository prior to paper acceptance.

## 716 **10 References**

717 Aitchison, J., & Meffre, S. (1992). New Caledonia: a tectonic collage in the southwest Pacific.  
718 In 29th International Geological Congress (Kyoto, 24 August-3 September 1992).

719 Alt, J., & Shanks III, W. (2006). Stable isotope compositions of serpentinite seamounts in the  
720 Mariana forearc: Serpentinization processes, fluid sources and sulfur metasomatism. *Earth and*  
721 *Planetary Science Letters*, 242(3-4), 272-285. <https://doi.org/10.1016/j.epsl.2005.11.063>

722 Alt, J. C., Schwarzenbach, E. M., Früh-Green, G. L., Shanks, W. C., Bernasconi, S. M., Garrido,  
723 C. J., et al. (2013). The role of serpentinites in cycling of carbon and sulfur: Seafloor  
724 serpentinization and subduction metamorphism. *Lithos*, 178, 40–54.  
725 <https://doi.org/10.1016/j.lithos.2012.12.006>

- 726 Angiboust, S., & Agard, P. (2010). Initial water budget: The key to detaching large volumes of  
727 eclogitized oceanic crust along the subduction channel? *Lithos*, 120(3–4), 453–474.  
728 <https://doi.org/10.1016/j.lithos.2010.09.007>
- 729 Auzende, A.-L., Daniel, I., Reynard, B., Lemaire, C., & Guyot, F. (2004). High-pressure  
730 behaviour of serpentine minerals: a Raman spectroscopic study. *Physics and Chemistry of*  
731 *Minerals*, 31(5), 269-277. <https://doi.org/10.1007/s00269-004-0384-0>
- 732 Bache, F., Mortimer, N., Sutherland, R., Collot, J., Rouillard, P., Stagpoole, V., & Nicol, A.  
733 (2014). Seismic stratigraphic record of transition from Mesozoic subduction to continental  
734 breakup in the Zealandia sector of eastern Gondwana. *Gondwana Research*, 26(3-4), 1060-1078.  
735 <https://doi.org/10.1016/j.gr.2013.08.012>
- 736 Baldwin, S. L., Rawling, T., & Fitzgerald, P. G. (2007). Thermochronology of the New  
737 Caledonian high-pressure terrane: Implications for middle Tertiary plate boundary processes in  
738 the southwest Pacific. *Convergent Margin Terranes and Associated Regions: A Tribute to W.G.*  
739 *Ernst*, 419(06), 117-134. [https://doi.org/10.1130/2006.2419\(06\)](https://doi.org/10.1130/2006.2419(06))
- 740 Barnes, I., & O'Neil, J. R. (1969). The relationship between fluids in some fresh Alpine-type  
741 ultramafics and possible modern serpentinization, Western United States. *GSA Bulletin*,  
742 80(October), 1947–1960. [https://doi.org/10.1130/0016-7606\(1969\)80\[1947:TRBFIS\]2.0.CO;2](https://doi.org/10.1130/0016-7606(1969)80[1947:TRBFIS]2.0.CO;2)
- 743 Barnes, J. D., Beltrando, M., Lee, C.-T. A., Cisneros, M., Loewy, S., & Chin, E. (2014).  
744 Geochemistry of Alpine serpentinites from rifting to subduction: A view across paleogeographic  
745 domains and metamorphic grade. *Chemical Geology*, 389, 29-47.  
746 <https://doi.org/10.1016/j.chemgeo.2014.09.012>
- 747 Barnes, J. D., Eldam, R., Lee, C.-T. A., Errico, J. C., Loewy, S., & Cisneros, M. (2013).  
748 Petrogenesis of serpentinites from the Franciscan Complex, western California, USA. *Lithos*,  
749 178, 143-157. <https://doi.org/10.1016/j.lithos.2012.12.018>
- 750 Barnes, J. D., Manning, C. E., Scambelluri, M., & Selverstone, J. (2018). The Behavior of  
751 Halogens During Subduction-Zone Processes. [https://doi.org/10.1007/978-3-319-61667-4\\_8](https://doi.org/10.1007/978-3-319-61667-4_8)

- 752 Bebout, G. E. (2007). Metamorphic chemical geodynamics of subduction zones. *Earth and*  
753 *Planetary Science Letters*, 260(3–4), 373–393. <https://doi.org/10.1016/j.epsl.2007.05.050>
- 754 Bebout, G. E., & Barton, M. D. (2002). Tectonic and metasomatic mixing in a high-T,  
755 subduction-zone mélange—insights into the geochemical evolution of the slab–mantle interface.  
756 *Chemical Geology*, 187(1–2), 79–106. [https://doi.org/10.1016/S0009-2541\(02\)00019-0](https://doi.org/10.1016/S0009-2541(02)00019-0)
- 757 Behr, W. M., & Bürgmann, R. (2021). What’s down there? The structures, materials and  
758 environment of deep-seated slow slip and tremor. *Philosophical Transactions of the Royal*  
759 *Society A: Mathematical, Physical and Engineering Sciences*, 379(2193), 20200218. [https://](https://doi.org/10.1098/rsta.2020.0218)  
760 [doi.org/10.1098/rsta.2020.0218](https://doi.org/10.1098/rsta.2020.0218)
- 761 Bhat, I. M., Ahmad, T., & Subba Rao, D. V. (2019). Origin and evolution of Suru Valley  
762 ophiolite peridotite slice along Indus suture zone, Ladakh Himalaya, India: Implications on melt-  
763 rock interaction in a subduction-zone environment. *Geochemistry*, 79(1), 78–93.  
764 <https://doi.org/10.1016/j.chemer.2018.10.003>
- 765 Black, P. M., & Brothers, R. N. (1977). Blueschist ophiolites in the melange zone, northern New  
766 Caledonia. *Contributions to Mineralogy and Petrology*, 65(1), 69–78. [https://doi.org/10.1007/B](https://doi.org/10.1007/BF00373572)  
767 [F00373572](https://doi.org/10.1007/BF00373572)
- 768 Black, P. M. (1993). Tectonism, magmatism and sedimentary basin development, Paleozoic to  
769 Paleogene, New Caledonia. *Bulletin of the Geological Society of Malaysia*, 33, 331–341.  
770 <https://doi.org/10.7186/bgsm33199323>
- 771 Blanco-Quintero, I. F., García-Casco, A., & Gerya, T. V. (2011). Tectonic blocks in serpentinite  
772 mélange (eastern Cuba) reveal large-scale convective flow of the subduction channel. *Geology*,  
773 39(1), 79–82. <https://doi.org/10.1130/G31494.1>
- 774 Bonatti, E. (1976). Serpentinite protrusions in the oceanic crust. *Earth and Planetary Science*  
775 *Letters*, 32(2), 107–113. [https://doi.org/10.1016/0012-821X\(76\)90048-0](https://doi.org/10.1016/0012-821X(76)90048-0)

- 776 Bostock, M. G., Hyndman, R. D., Rondenay, S., & Peacock, S. M. (2002). An inverted  
777 continental Moho and serpentinization of the forearc mantle. *Nature*, 417(6888), 536–538.  
778 <https://doi.org/10.1038/417536a>
- 779 Brothers, R. N. (1974). High-pressure schists in Northern New Caledonia. *Contributions to*  
780 *Mineralogy and Petrology*, 46(2), 109–127. <https://doi.org/10.1007/BF00377499>
- 781 Brothers, R. N., & Blake, M. C. (1973). Tertiary plate tectonics and high-pressure  
782 metamorphism in New Caledonia. *Tectonophysics*, 17(4), 337–358.  
783 [https://doi.org/10.1016/0040-1951\(73\)90046-2](https://doi.org/10.1016/0040-1951(73)90046-2)
- 784 Burkhard, D. J. M., & O’Neil, J. R. (1988). Contrasting serpentinization processes in the eastern  
785 Central Alps. *Contributions to Mineralogy and Petrology*, 99(4), 498–506.  
786 <https://doi.org/10.1007/BF00371940>
- 787 Campbell, H. J., Grant-Mackie, J. A., & Paris, J. P. (1985). Geology of the Moindou-Teremba  
788 area, New Caledonia. Stratigraphy and structure of Teremba Group (Permian-Lower Triassic)  
789 and Baie de St.-Vincent Group (Upper Triassic- Lower Jurassic). *Géologie de la France*, 1, 19-  
790 36.
- 791 Cannà, E., Scambelluri, M., Agostini, S., Tonarini, S., & Godard, M. (2016). Linking  
792 serpentinite geochemistry with tectonic evolution at the subduction plate-interface: The Voltri  
793 Massif case study (Ligurian Western Alps, Italy). *Geochimica et Cosmochimica Acta*, 190, 115–  
794 133. <https://doi.org/10.1016/j.gca.2016.06.034>
- 795 Cannat, M. (1993). Emplacement of mantle rocks in the seafloor at mid-ocean ridges. *Journal of*  
796 *Geophysical Research: Solid Earth*, 98(B3), 4163–4172. <https://doi.org/10.1029/92JB02221>
- 797 Cannat, M., Fontaine, F., & Escartín, J. (2010). Serpentinization and associated hydrogen and  
798 methane fluxes at slow spreading ridges. In P. A. Rona, C. W. Devey, J. Dymant, & B. J. Murton  
799 (Eds.), *Diversity of Hydrothermal Systems on Slow Spreading Ocean Ridges* (pp. 241–264).  
800 American Geophysical Union. <https://doi.org/10.1029/2008GM000760>

- 801 Cárdenas-Párraga, J., García-Casco, A., Proenza, J. A., Harlow, G. E., Blanco-Quintero, I. F.,  
802 Lázaro, C., et al. (2017). Trace-element geochemistry of transform-fault serpentinite in high-  
803 pressure subduction mélanges (eastern Cuba): implications for subduction initiation. *International*  
804 *Geology Review*, 59(16), 2041-2064. <https://doi.org/10.1080/00206814.2017.1308843>
- 805 Clarke, G. L., Aitchison, J. C., & Cluzel, D. (1997). Eclogites and Blueschists of the Pam  
806 Peninsula, NE New Caledonia: a Reappraisal. *Journal of Petrology*, 38(7), 843–876.  
807 <https://doi.org/10.1093/petroj/38.7.843>
- 808 Cloos, M., & Shreve, R. L. (1988). Subduction-channel model of prism accretion, melange  
809 formation, sediment subduction, and subduction erosion at convergent plate margins: 1.  
810 Background and description. *Pure and Applied Geophysics PAGEOPH*, 128(3–4), 455–500.  
811 <https://doi.org/10.1007/BF00874548>
- 812 Cluzel, D., Adams, C. J., Meffre, S., Campbell, H., & Maurizot, P. (2010). Discovery of Early  
813 Cretaceous Rocks in New Caledonia: New Geochemical and U-Pb Zircon Age Constraints on  
814 the Transition from Subduction to Marginal Breakup in the Southwest Pacific. *The Journal of*  
815 *Geology*, 118(4), 381–397. <https://doi.org/10.1086/652779>
- 816 Cluzel, D. (2021). Subduction erosion: contributions of footwall and hanging wall to serpentinite  
817 mélange; field, geochemical and radiochronological evidence from the Eocene HP-LT belt of  
818 New Caledonia. *Australian Journal of Earth Sciences*, 68(1), 99-119.  
819 <https://doi.org/10.1080/08120099.2020.1761876>
- 820 Cluzel, D., Aitchison, J. C., Clarke, G. L., Meffre, S., & Picard, C. (1994). Point de vue sur  
821 l'évolution tectonique et géodynamique de la Nouvelle-Calédonie (Pacifique, France). *Comptes*  
822 *Rendus De L'Académie Des Sciences. Série II. Fascicule A, Sciences De La Terre Et Des*  
823 *Planètes*, 319(6), 683-690.
- 824 Cluzel, D., Aitchison, J. C., Clarke, G. L., Meffre, S., & Picard, C. (1995). Dénudation  
825 tectonique du complexe à noyau métamorphique de haute pression d'âge tertiaire (Nord de la  
826 Nouvelle-Calédonie, Pacifique, France). *Comptes Rendus De L'Académie Des Sciences. Série II.*  
827 *Fascicule A, Sciences De La Terre Et Des Planètes*, 321(1), 57-64.

- 828 Cluzel, D., Boulvais, P., Iseppi, M., Lahondère, D., Lesimple, S., Maurizot, P., et al. (2020).  
829 Slab-derived origin of tremolite–antigorite veins in a supra-subduction ophiolite: the Peridotite  
830 Nappe (New Caledonia) as a case study. *International Journal of Earth Sciences*, 109(1), 171-  
831 196. <https://doi.org/10.1007/s00531-019-01796-6>
- 832 Cluzel, D., Jourdan, F., Meffre, S., Maurizot, P., & Lesimple, S. (2012). The metamorphic sole  
833 of New Caledonia ophiolite: 40 Ar/ 39 Ar, U-Pb, and geochemical evidence for subduction  
834 inception at a spreading ridge. *Tectonics*, 31(3). <https://doi.org/10.1029/2011TC003085>
- 835 Cluzel, D., & Meffre, S. (2002). L'unité de la Boghen (Nouvelle-Calédonie, Pacifique sud-  
836 ouest): Un complexe d'accrétion jurassique. Données radiochronologiques préliminaires U-Pb  
837 sur les zircons détritiques. *Comptes Rendus - Geoscience*, 334(11), 867–874.  
838 [https://doi.org/10.1016/S1631-0713\(02\)01823-0](https://doi.org/10.1016/S1631-0713(02)01823-0)
- 839 Cluzel, D., Meffre, S., Maurizot, P., & Crawford, A. J. (2006). Earliest Eocene (53 Ma)  
840 convergence in the Southwest Pacific: evidence from pre-obduction dikes in the ophiolite of  
841 New Caledonia. *Terra Nova*, 18(6), 395-402. <https://doi.org/10.1111/j.1365-3121.2006.00704.x>
- 842 Cluzel, D., Ulrich, M., Jourdan, F., Meffre, S., Paquette, J.-L., Audet, M.-A., et al. (2016). Early  
843 Eocene clinoenstatite boninite and boninite-series dikes of the ophiolite of New Caledonia; a  
844 witness of slab-derived enrichment of the mantle wedge in a nascent volcanic arc. *Lithos*, 260,  
845 429-442. <https://doi.org/10.1016/j.lithos.2016.04.031>
- 846 Codillo, E. A., Le Roux, V., & Marschall, H. R. (2018). Arc-like magmas generated by mélange-  
847 peridotite interaction in the mantle wedge. *Nature Communications*, 9(1), 2864.  
848 <https://doi.org/10.1038/s41467-018-05313-2>
- 849 Coleman, R. G. (1967). Glaucophane schists from California and New Caledonia.  
850 *Tectonophysics*, 4(4–6), 479–498. [https://doi.org/10.1016/0040-1951\(67\)90012-1](https://doi.org/10.1016/0040-1951(67)90012-1)
- 851 Collins, N. C., Bebout, G. E., Angiboust, S., Agard, P., Scambelluri, M., Crispini, L., & John, T.  
852 (2015). Subduction zone metamorphic pathway for deep carbon cycling: II. Evidence from

- 853 HP/UHP metabasaltic rocks and ophicarbonates. *Chemical Geology*, 412, 132-150.  
854 <https://doi.org/10.1016/j.chemgeo.2015.06.012>
- 855 Collot, J. Y., Malahoff, A., Recy, J., Latham, G., & Missegue, F. (1987). Overthrust  
856 emplacement of New Caledonia Ophiolite: Geophysical evidence. *Tectonics*, 6(3), 215–232.  
857 <https://doi.org/10.1029/TC006i003p00215>
- 858 Cooperdock, E. H. G., Raia, N. H., Barnes, J. D., Stockli, D. F., & Schwarzenbach, E. M. (2018).  
859 Tectonic origin of serpentinites on Syros, Greece: Geochemical signatures of abyssal origin  
860 preserved in a HP/LT subduction complex. *Lithos*, 296–299(January), 352–364.  
861 <https://doi.org/10.1016/j.lithos.2017.10.020>
- 862 Cooperdock, E. H. G., & Stockli, D. F. (2016). Unraveling alteration histories in serpentinites  
863 and associated ultramafic rocks with magnetite (U-Th)/He geochronology. *Geology*, 44(11),  
864 967–970. <https://doi.org/10.1130/G38587.1>
- 865 Crawford, A. J., Meffre, S., & Symonds, P. A. (2003). 120 to 0 Ma tectonic evolution of the  
866 southwest Pacific and analogous geological evolution of the 600 to 220 Ma Tasman Fold Belt  
867 System. In *Evolution and Dynamics of the Australian Plate*, 22, 383-403.  
868 <https://doi.org/10.1130/0-8137-2372-8.383>
- 869 Davies, H. L., & Smith, I. E. (1971). *Geology of eastern Papua*. Geological Society of America  
870 *Bulletin*, 82(12), 3299-3312.
- 871 Debret, B., Albers, E., Walter, B., Price, R., Barnes, J. D., Beunon, H., et al. (2019). Shallow  
872 forearc mantle dynamics and geochemistry: New insights from IODP Expedition 366. *Lithos*,  
873 326-327, 230-245. <https://doi.org/10.1016/j.lithos.2018.10.038>
- 874 Debret, B., Reekie, C. D. J., Mattielli, N., Beunon, H., Ménez, B., Savov, I., & Williams, H. M.  
875 (2020). Redox transfer at subduction zones: insights from Fe isotopes in the Mariana forearc.  
876 *Geochemical Perspective Letters*, 46-51. <https://doi.org/10.7185/geochemlet.2003>

- 877 Debret, B., & Sverjensky, D. A. (2017). Highly oxidising fluids generated during serpentinite  
878 breakdown in subduction zones. *Scientific Reports*, 7(1), 10351. [https://doi.org/10.1038/s41598-](https://doi.org/10.1038/s41598-017-09626-y)  
879 017-09626-y
- 880 Deschamps, F., Godard, M., Guillot, S., & Hattori, K. (2013). Geochemistry of subduction zone  
881 serpentinites: A review. *Lithos*, 178, 96–127. <https://doi.org/10.1016/j.lithos.2013.05.019>
- 882 Deschamps, F., Guillot, S., Godard, M., Andreani, M., & Hattori, K. (2011). Serpentinites act as  
883 sponges for fluid-mobile elements in abyssal and subduction zone environments. *Terra Nova*,  
884 23(3), 171-178. <https://doi.org/10.1111/j.1365-3121.2011.00995.x>
- 885 Deschamps, F., Guillot, S., Godard, M., Chauvel, C., Andreani, M., & Hattori, K. (2010). In situ  
886 characterization of serpentinites from forearc mantle wedges: Timing of serpentinization and  
887 behavior of fluid-mobile elements in subduction zones. *Chemical Geology*, 269(3-4), 262-277.  
888 <https://doi.org/10.1016/j.chemgeo.2009.10.002>
- 889 Dubois, J., Launay, J., & Recy, J. (1974). Uplift movements in New Caledonia-Loyalty Islands  
890 area and their plate tectonics interpretation. *Tectonophysics*, 24(1–2), 133–150.  
891 [https://doi.org/10.1016/0040-1951\(74\)90134-6](https://doi.org/10.1016/0040-1951(74)90134-6)
- 892 Dupuy, C., Dostal, J., & Leblanc, M. (1981). Geochemistry of an ophiolitic complex from New  
893 Caledonia. *Contributions to Mineralogy and Petrology*, 76(1), 77–83.  
894 <https://doi.org/10.1007/BF00373686>
- 895 Eiler, J. M. (2001). 5. Oxygen Isotope Variations of Basaltic Lavas and Upper Mantle Rocks. In  
896 *Stable Isotope Geochemistry* (Vol. 43, pp. 319–364). De Gruyter.  
897 <https://doi.org/10.1515/9781501508745-008>
- 898 Evans, K. A. (2012). The redox budget of subduction zones. *Earth-Science Reviews*, 113(1–2),  
899 11–32. <https://doi.org/10.1016/j.earscirev.2012.03.003>
- 900 Evans, K. A., Reddy, S. M., Tomkins, A. G., Crossley, R. J., & Frost, B. R. (2017). Effects of  
901 geodynamic setting on the redox state of fluids released by subducted mantle lithosphere. *Lithos*,  
902 278-281, 26-42. <https://doi.org/10.1016/j.lithos.2016.12.023>

- 903 Evans, K. A., & Frost, B. R. (2021). Deserpentinization in Subduction Zones as a Source of  
904 Oxidation in Arcs: a Reality Check. *Journal of Petrology*, 62(3), 1–32.  
905 <https://doi.org/10.1093/petrology/egab016>
- 906 Ferrand, T. P. (2019). Seismicity and mineral destabilizations in the subducting mantle up to 6  
907 GPa, 200 km depth. *Lithos*, 334–335, 205–230. <https://doi.org/10.1016/j.lithos.2019.03.014>
- 908 Fitzherbert, J. A., Clarke, G. L., & Powell, R. (2003). Lawsonite-Omphacite-Bearing  
909 Metabasites of the Pam Peninsula, NE New Caledonia: Evidence for Disrupted Blueschist- to  
910 Eclogite-Facies Conditions. *Journal of Petrology*, 44(10), 1805-1831.  
911 <https://doi.org/10.1093/petrology/egg060>
- 912 Fitzherbert, J. A., Clarke, G. L., Marmo, B., & Powell, R. (2004). The origin and P-T evolution  
913 of peridotites and serpentinites of NE New Caledonia: prograde interaction between continental  
914 margin and the mantle wedge. *Journal of Metamorphic Geology*, 22(4), 327-344.  
915 <https://doi.org/10.1111/j.1525-1314.2004.00517.x>
- 916 Früh-Green, G. L., Scambelluri, M., & Vallis, F. (2001). O–H isotope ratios of high pressure  
917 ultramafic rocks: implications for fluid sources and mobility in the subducted hydrous mantle.  
918 *Contributions to Mineralogy and Petrology*, 141(2), 145-159.  
919 <https://doi.org/10.1007/s004100000228>
- 920 Früh-Green, G. L., Weissert, H., & Bernoulli, D. (1990). A multiple fluid history recorded in  
921 Alpine ophiolites. *Journal of the Geological Society*, 147(6), 959–970.  
922 <https://doi.org/10.1144/gsjgs.147.6.0959>
- 923 Fyfe, W., & McBirney, A. (1975). Subduction and the structure of andesitic volcanic belts.  
924 *American Journal of Science*, Vol. 275-A, pp. 285–297.
- 925 Gautier, P., Quesnel, B., Boulvais, P., & Cathelineau, M. (2016). The emplacement of the  
926 Peridotite Nappe of New Caledonia and its bearing on the tectonics of obduction. *Tectonics*,  
927 35(12), 3070–3094. <https://doi.org/10.1002/2016TC004318>

- 928 Gerya, T. V., Stöckhert, B., & Perchuk, A. L. (2002). Exhumation of high-pressure metamorphic  
929 rocks in a subduction channel: A numerical simulation. *Tectonics*, 21(6), 6-1-6–19.  
930 <https://doi.org/10.1029/2002TC001406>
- 931 Gerya, T., & Stöckhert, B. (2006). Two-dimensional numerical modeling of tectonic and  
932 metamorphic histories at active continental margins. *International Journal of Earth Sciences*,  
933 95(2), 250–274. <https://doi.org/10.1007/s00531-005-0035-9>
- 934 Groppo, C., Rinaudo, C., Cairo, S., Gastaldi, D., & Compagnoni, R. (2006). Micro-Raman  
935 spectroscopy for a quick and reliable identification of serpentine minerals from ultramafics.  
936 *European Journal of Mineralogy*, 18(3), 319-329. [https://doi.org/10.1127/0935-1221/2006/0018-](https://doi.org/10.1127/0935-1221/2006/0018-0319)  
937 0319
- 938 Guérangé, B., Lozes, J., Autran, A., 1977. Mesozoic metamorphism in the New Caledonia  
939 central chain and its geodynamic implications in relation to the evolution of the Cretaceous  
940 Rangitata Orogeny. In: *International Symposium on Geodynamics in South-West Pacific* (pp.  
941 265–278). Paris: Technip.
- 942 Guice, G. L., Ackerson, M. R., Holder, R. M., George, F. R., Browning-Hanson, J. F., Burgess,  
943 J. L., et al. (2021). Suprasubduction zone ophiolite fragments in the central Appalachian orogen:  
944 Evidence for mantle and Moho in the Baltimore Mafic Complex (Maryland, USA). *Geosphere*,  
945 17(2), 561-581. <https://doi.org/10.1130/GES02289.1>
- 946 Guillot, S., Hattori, K. H., & de Sigoyer, J. (2000). Mantle wedge serpentization and  
947 exhumation of eclogites: Insights from eastern Ladakh, northwest Himalaya. *Geology*, 28(3),  
948 199–202. [https://doi.org/10.1130/0091-7613\(2000\)028<0199:MWSAEO>2.3.CO;2](https://doi.org/10.1130/0091-7613(2000)028<0199:MWSAEO>2.3.CO;2)
- 949 Guillot, S., Hattori, K., Agard, P., Schwartz, S., & Vidal, O. (2009). Exhumation Processes in  
950 Oceanic and Continental Subduction Contexts: A Review. In: Lallemand S., Funiciello F. (eds)  
951 *Subduction Zone Geodynamics*. *Frontiers in Earth Sciences*. Springer, Berlin, Heidelberg.  
952 [https://doi.org/10.1007/978-3-540-87974-9\\_10](https://doi.org/10.1007/978-3-540-87974-9_10)

- 953 Guillot, S., Schwartz, S., Reynard, B., Agard, P., & Prigent, C. (2015). Tectonic significance of  
954 serpentinites. *Tectonophysics*, 646(February), 1–19. <https://doi.org/10.1016/j.tecto.2015.01.020>
- 955 Hacker, B. R., Peacock, S. M., Abers, G. A., & Holloway, S. D. (2003). Subduction factory 2.  
956 Are intermediate-depth earthquakes in subducting slabs linked to metamorphic dehydration  
957 reactions? *Journal of Geophysical Research: Solid Earth*, 108(B1).  
958 <https://doi.org/10.1029/2001JB001129>
- 959 Hacker, B. R. (2008). H<sub>2</sub>O subduction beyond arcs. *Geochemistry, Geophysics, Geosystems*,  
960 9(3), Q03001. <https://doi.org/10.1029/2007GC001707>
- 961 Halama, R., Bebout, G. E., John, T., & Scambelluri, M. (2014). Nitrogen recycling in subducted  
962 mantle rocks and implications for the global nitrogen cycle. *International Journal of Earth  
963 Sciences*, 103(7), 2081–2099. <https://doi.org/10.1007/s00531-012-0782-3>
- 964 Hart, S. R., & Zindler, A. (1986). In search of a bulk-Earth composition. *Chemical Geology*,  
965 57(3–4), 247–267. [https://doi.org/10.1016/0009-2541\(86\)90053-7](https://doi.org/10.1016/0009-2541(86)90053-7)
- 966 Hattori, K. H., & Guillot, S. (2003). Volcanic fronts form as a consequence of serpentinite  
967 dehydration in the forearc mantle wedge. *Geology*, 31(6), 525. [https://doi.org/10.1130/0091-  
7613\(2003\)031<0525:VFFAAC>2.0.CO;2](https://doi.org/10.1130/0091-<br/>968 7613(2003)031<0525:VFFAAC>2.0.CO;2)
- 969 Hattori, K., Wallis, S., Enami, M., & Mizukami, T. (2010). Subduction of mantle wedge  
970 peridotites: Evidence from the Higashi-akaishi ultramafic body in the Sanbagawa metamorphic  
971 belt. *Island Arc*, 19(1), 192–207. <https://doi.org/10.1111/j.1440-1738.2009.00696.x>
- 972 Hermann, J., Müntener, O., & Scambelluri, M. (2000). The importance of serpentinite mylonites  
973 for subduction and exhumation of oceanic crust. *Tectonophysics*, 327(3–4), 225–238.  
974 [https://doi.org/10.1016/S0040-1951\(00\)00171-2](https://doi.org/10.1016/S0040-1951(00)00171-2)
- 975 Hilaiet, N., Daniel, I., & Reynard, B. (2006). Equation of state of antigorite, stability field of  
976 serpentines, and seismicity in subduction zones. *Geophysical Research Letters*, 33(2), L02302.  
977 <https://doi.org/10.1029/2005GL024728>

- 978 Hilairret, N., & Reynard, B. (2009). Stability and dynamics of serpentinite layer in subduction  
979 zone. *Tectonophysics*, 465(1–4), 24–29. <https://doi.org/10.1016/j.tecto.2008.10.005>
- 980 Hilairret, N., Reynard, B., Wang, Y., Daniel, I., Merkel, S., Nishiyama, N., & Petitgirard, S.  
981 (2007). High-Pressure Creep of Serpentine, Interseismic Deformation, and Initiation of  
982 Subduction. *Science*, 318(5858), 1910–1913. <https://doi.org/10.1126/science.1148494>
- 983 Hirth, G., & Guillot, S. (2013). Rheology and Tectonic Significance of Serpentinite. *Elements*,  
984 9(2), 107–113. <https://doi.org/10.2113/gselements.9.2.107>
- 985 Hyndman, R. D., & Peacock, S. M. (2003). Serpentinization of the forearc mantle. *Earth and*  
986 *Planetary Science Letters*, 212(3–4), 417–432. [https://doi.org/10.1016/S0012-821X\(03\)00263-2](https://doi.org/10.1016/S0012-821X(03)00263-2)
- 987 Jagoutz, E., Palme, H., Baddenhausen, H., Blum, K., Cendales, M., Dreibus, G., et al. (1979).  
988 The abundance of major, minor and trace elements in the earth's mantle as derived from  
989 primitive ultramafic nodules. *Lunar and Planetary Science Conference Proceedings*, 10, 2031–  
990 2050.
- 991 John, T., Scambelluri, M., Frische, M., Barnes, J. D., & Bach, W. (2011). Dehydration of  
992 subducting serpentinite: Implications for halogen mobility in subduction zones and the deep  
993 halogen cycle. *Earth and Planetary Science Letters*, 308(1–2), 65–76.  
994 <https://doi.org/10.1016/j.epsl.2011.05.038>
- 995 Johnson, D., Hooper, P., & Conrey, R. (1999). XRF method XRF analysis of rocks and minerals  
996 for major and trace elements on a single low dilution Li-tetraborate fused bead. *Advances in X-*  
997 *ray Analysis*, 41, 843-867.
- 998 Jung, H., & Green, H. W. (2004). Experimental Faulting of Serpentinite during Dehydration:  
999 Implications for Earthquakes, Seismic Low-Velocity Zones, and Anomalous Hypocenter  
1000 Distributions in Subduction Zones. *International Geology Review*, 46(12), 1089-1102.  
1001 <https://doi.org/10.2747/0020-6814.46.12.1089>
- 1002 Katzir, Y., Avigad, D., Matthews, A., Garfunkel, Z., & Evans, B. W. (2000). Origin, HP/LT  
1003 metamorphism and cooling of ophiolitic mélanges in southern Evia (NW Cyclades), Greece.

- 1004 Journal of Metamorphic Geology, 18(6), 699-718. <https://doi.org/10.1046/j.1525->  
1005 1314.2000.00281.x
- 1006 Kelly, D. S. (2018). Analysis of Geological Materials by Low Dilution Fusion at the Peter  
1007 Hooper GeoAnalytical Lab (Washington State University). Washington State University,  
1008 Pullman, WA, USA.
- 1009 Kendrick, M. A., Hémond, C., Kamenetsky, V. S., Danyushevsky, L., Devey, C. W., Rodemann,  
1010 T., et al. (2017). Seawater cycled throughout Earth's mantle in partially serpentinized  
1011 lithosphere. *Nature Geoscience*, 10(3), 222-228. <https://doi.org/10.1038/ngeo2902>
- 1012 Kendrick, M. A., Scambelluri, M., Honda, M., & Phillips, D. (2011). High abundances of noble  
1013 gas and chlorine delivered to the mantle by serpentinite subduction. *Nature Geoscience*, 4(11),  
1014 807-812. <https://doi.org/10.1038/ngeo1270>
- 1015 Kerrick, D. M., & Connolly, J. A. D. (1998). Subduction of ophiicarbonates and recycling of CO<sub>2</sub>  
1016 and H<sub>2</sub>O. *Geology*, 26(4), 375-378. <https://doi.org/10.1130/0091->  
1017 7613(1998)026<0375:SOOARO>2.3.CO;2
- 1018 Kerswell, B. C., Kohn, M. J., & Gerya, T. V. (2021). Backarc Lithospheric Thickness and  
1019 Serpentine Stability Control Slab-Mantle Coupling Depths in Subduction Zones. *Geochemistry,*  
1020 *Geophysics, Geosystems*, 22(6). <https://doi.org/10.1029/2020GC009304>
- 1021 Klingelhofer, F., Lafoy, Y., Collot, J., Cosquer, E., Géli, L., Nouzé, H., & Vially, R. (2007).  
1022 Crustal structure of the basin and ridge system west of New Caledonia (southwest Pacific) from  
1023 wide-angle and reflection seismic data. *Journal of Geophysical Research*, 112(B11), B11102.  
1024 <https://doi.org/10.1029/2007JB005093>
- 1025 Knaack, C. M., Cornelius, S., & Hooper, P. R. (1994). Trace element analysis of rocks and  
1026 minerals by ICP-MS: Washington State University. Geology Department, Open File Report.
- 1027 Kodolányi, J., Pettke, T., Spandler, C., Kamber, B. S., & Gméling, K. (2012). Geochemistry of  
1028 Ocean Floor and Fore-arc Serpentinites: Constraints on the Ultramafic Input to Subduction  
1029 Zones. *Journal of Petrology*, 53(2), 235-270. <https://doi.org/10.1093/petrology/egr058>

- 1030 Kyser, T. K., O’Hanley, D. S., & Wicks, F. J. (1999). The origin of fluids associated with  
1031 serpentinization processes: Evidence from stable-isotope compositions. *Canadian Mineralogist*,  
1032 37(1), 223–237.
- 1033 Kyser, T. K., & O’Neil, J. R. (1984). Hydrogen isotope systematics of submarine basalts.  
1034 *Geochimica et Cosmochimica Acta*, 48(10), 2123–2133. [https://doi.org/10.1016/0016-](https://doi.org/10.1016/0016-7037(84)90392-2)  
1035 7037(84)90392-2
- 1036 Lafoy, Y., Brodien, I., Vially, R., & Exon, N. F. (2005). Structure of the Basin and Ridge System  
1037 West of New Caledonia (Southwest Pacific): A Synthesis. *Marine Geophysical Researches*,  
1038 26(1), 37-50. <https://doi.org/10.1007/s11001-005-5184-5>
- 1039 Lazar, C., Cooperdock, E. H. G., & Seymour, B. H. T. (2021). A continental forearc serpentinite  
1040 diapir with deep origins: Elemental signatures of a mantle wedge protolith and slab-derived  
1041 fluids at New Idria, California. *Lithos*, 398-399, 106252.  
1042 <https://doi.org/10.1016/j.lithos.2021.106252>
- 1043 Li, H.-Y., Chen, R.-X., Zheng, Y.-F., Hu, Z., & Xu, L. (2018). Crustal Metasomatism at the  
1044 Slab-Mantle Interface in a Continental Subduction Channel: Geochemical Evidence From  
1045 Orogenic Peridotite in the Sulu Orogen. *Journal of Geophysical Research: Solid Earth*, 123(3),  
1046 2174–2198. <https://doi.org/10.1002/2017JB014015>
- 1047 Li, X.-P., Rahn, M., & Bucher, K. (2004). Serpentinites of the Zermatt-Saas ophiolite complex  
1048 and their texture evolution. *Journal of Metamorphic Geology*, 22(3), 159–177.  
1049 <https://doi.org/10.1111/j.1525-1314.2004.00503.x>
- 1050 Lillie, A. (1975). Structures in the lawsonite—glaucophane schists of New  
1051 Caledonia. *Geological Magazine*, 112(3), 225-240. <https://doi.org/10.1017/S0016756800046999>
- 1052 Liu, C.-Z., Xu, Y., & Wu, F.-Y. (2018). Limited recycling of crustal osmium in forearc mantle  
1053 during slab dehydration. *Geology*, 46(3), 239–242. <https://doi.org/10.1130/G39869.1>
- 1054 Magott, R., Fabbri, O., & Fournier, M. (2020). Seismically-induced serpentine dehydration as a  
1055 possible mechanism of water release in subduction zones. Insights from the Alpine Corsica

- 1056 pseudotachylyte-bearing Monte Maggiore ophiolitic unit. *Lithos*, 362-363, 105474.  
1057 <https://doi.org/10.1016/j.lithos.2020.105474>
- 1058 Malatesta, C., Gerya, T., Scambelluri, M., Federico, L., Crispini, L., & Capponi, G. (2012).  
1059 Intraoceanic subduction of “heterogeneous” oceanic lithosphere in narrow basins: 2D numerical  
1060 modeling. *Lithos*, 140–141, 234–251. <https://doi.org/10.1016/j.lithos.2012.01.003>
- 1061 Malvoisin, B. (2015). Mass transfer in the oceanic lithosphere: Serpentinization is not  
1062 isochemical. *Earth and Planetary Science Letters*, 430, 75–85.  
1063 <https://doi.org/10.1016/j.epsl.2015.07.043>
- 1064 Marchesi, C., Garrido, C. J., Godard, M., Belley, F., & Ferré, E. (2009). Migration and  
1065 accumulation of ultra-depleted subduction-related melts in the Massif du Sud ophiolite (New  
1066 Caledonia). *Chemical Geology*, 266(3-4), 171-186.  
1067 <https://doi.org/10.1016/j.chemgeo.2009.06.004>
- 1068 Marschall, H. R., & Schumacher, J. C. (2012). Arc magmas sourced from mélange diapirs in  
1069 subduction zones. *Nature Geoscience*, 5(12), 862–867. <https://doi.org/10.1038/ngeo1634>
- 1070 Matthey, D., Lowry, D., & Macpherson, C. (1994). Oxygen isotope composition of mantle  
1071 peridotite. *Earth and Planetary Science Letters*, 128(3–4), 231–241.  
1072 [https://doi.org/10.1016/0012-821X\(94\)90147-3](https://doi.org/10.1016/0012-821X(94)90147-3)
- 1073 Maurizot, P. (2011). First sedimentary record of the pre-obduction convergence in New  
1074 Caledonia: formation of an Early Eocene accretionary complex in the north of Grande Terre and  
1075 emplacement of the ‘Montagnes Blanches’ nappe. *Bulletin de la Société Géologique de France*,  
1076 182(6), 479-491. <https://doi.org/10.2113/gssgfbull.182.6.479>
- 1077 Maurizot, P. & Collot, J. (2009). Explanatory note of the geological map of New Caledonia,  
1078 scale 1/500,000. Direction de l’Industrie, des Mines et de l’Energie – Service géologique de  
1079 Nouvelle Calédonie, Bureau de Recherches Géologiques et Minières.

- 1080 Maurizot, P., Eberle, J-M, Habault, C. & Tessarollo, C. (1989). Carte géologique á l'échelle du  
1081 1/50,000 et notice explicative sur la feuille Pam-Ouégoa, 2nd edn. Nouméa, New Caledonia:  
1082 Bureau de Recherches Geologique et Mineres.
- 1083 Maurizot, P., Robineau, B., Vendé-Leclerc, M., & Cluzel, D. (2020a). Introduction to New  
1084 Caledonia: geology, geodynamic evolution and mineral resources. Geological Society, London,  
1085 *Memoirs*, 51(1), 1-12. <https://doi.org/10.1144/M51>
- 1086 Maurizot, P., Cluzel, D., Meffre, S., Campbell, H. J., Collot, J., & Sevin, B. (2020b). Chapter 3  
1087 Pre-Late Cretaceous basement terranes of the Gondwana active margin of New Caledonia.  
1088 Geological Society, London, *Memoirs*, 51(1), 27-52. <https://doi.org/10.1144/M51-2016-11>
- 1089 Maurizot, P., Cluzel, D., Patriat, M., Collot, J., Iseppi, M., Lesimple, S., et al. (2020c). Chapter 5  
1090 The Eocene Subduction–Obduction Complex of New Caledonia. Geological Society, London,  
1091 *Memoirs*, 51(1), 93-130. <https://doi.org/10.1144/M51-2018-70>
- 1092 McDonough, W. F., & Sun, S. -s. (1995). The composition of the Earth. *Chemical Geology*,  
1093 120(3–4), 223–253. [https://doi.org/10.1016/0009-2541\(94\)00140-4](https://doi.org/10.1016/0009-2541(94)00140-4)
- 1094 Meffre, S., Aitchison, J. C., & Crawford, A. J. (1996). Geochemical stratigraphy of boninites and  
1095 tholeiites from the Permo-Triassic Koh Ophiolite, New Caledonia. *Tectonics*, 15(1), 67–83.
- 1096 Mével, C. (2003). Serpentinization of abyssal peridotites at mid-ocean ridges. *Comptes Rendus*  
1097 *Geoscience*, 335(10–11), 825–852. <https://doi.org/10.1016/j.crte.2003.08.006>
- 1098 Mortimer, N., Gans, P. B., Meffre, S., Martin, C. E., Seton, M., Williams, S., ... Rollet, N.  
1099 (2018). Regional volcanism of northern Zealandia: post-Gondwana break-up magmatism on an  
1100 extended, submerged continent. Geological Society, London, *Special Publications*, 463(1), 199-  
1101 226. <https://doi.org/10.1144/SP463.9>
- 1102 Mortimer, N., Campbell, H. J., Tulloch, A. J., King, P. R., Stagpoole, V. M., Wood, R. A., ...  
1103 Seton, M. (2017). Zealandia: Earth's Hidden Continent. *GSA Today*, 27(3–4), 27–35.  
1104 <https://doi.org/10.1130/GSATG321A.1>

- 1105 Mothersole, F. E. (2014). A Comparative Study of Progressive Serpentinisation. Curtin  
1106 University.
- 1107 Mothersole, F. E., Evans, K., & Frost, B. R. (2017). Abyssal and hydrated mantle wedge  
1108 serpentinised peridotites: A comparison of the 15°20'N fracture zone and New Caledonia  
1109 serpentinites. *Contributions to Mineralogy and Petrology*, 172(8), 69.  
1110 <https://doi.org/10.1007/s00410-017-1381-x>
- 1111 Moutte, J. (1982). Chromite deposits of the Tiebaghi ultramafic massif, New Caledonia.  
1112 *Economic Geology*, 77(3), 576–591. <https://doi.org/10.2113/gsecongeo.77.3.576>
- 1113 Nielsen, S. G., & Marschall, H. R. (2017). Geochemical evidence for mélange melting in global  
1114 arcs. *Science Advances*, 3(4), 1–7. <https://doi.org/10.1126/sciadv.1602402>
- 1115 Niu, Y. (2004). Bulk-rock Major and Trace Element Compositions of Abyssal Peridotites:  
1116 Implications for Mantle Melting, Melt Extraction and Post-melting Processes Beneath Mid-  
1117 Ocean Ridges. *Journal of Petrology*, 45(12), 2423-2458.  
1118 <https://doi.org/10.1093/petrology/egh068>
- 1119 Paris, J. P. (1981). Géologie de la Nouvelle-Calédonie, un essai de synthèse. Mémoires du  
1120 Bureau de Recherches Géologiques et Minières, 113.
- 1121 Parkinson, I. J., & Pearce, J. A. (1998). Peridotites from the Izu-Bonin-Mariana Forearc (ODP  
1122 Leg 125): Evidence for Mantle Melting and Melt-Mantle Interaction in a Supra-Subduction Zone  
1123 Setting. *Journal of Petrology*, 39(9), 1577–1618. <https://doi.org/10.1093/etroj/39.9.1577>
- 1124 Patriat, M., Collot, J., Etienne, S., Poli, S., Clerc, C., Mortimer, N., ... Roest, W. R. (2018). New  
1125 Caledonia Obducted Peridotite Nappe: Offshore Extent and Implications for Obduction and  
1126 Postobduction Processes. *Tectonics*, 37(4), 1077-1096. <https://doi.org/10.1002/2017TC004722>
- 1127 Peacock, S. M., & Hyndman, R. D. (1999). Hydrous minerals in the mantle wedge and the  
1128 maximum depth of subduction thrust earthquakes. *Geophysical Research Letters*, 26(16), 2517–  
1129 2520. <https://doi.org/10.1029/1999GL900558>

- 1130 Peacock, S. M. (2001). Are the lower planes of double seismic zones caused by serpentine  
1131 dehydration in subducting oceanic mantle? *Geology*, 29(4), 299. [https://doi.org/10.1130/0091-7613\(2001\)029<0299:ATLPOD>2.0.CO;2](https://doi.org/10.1130/0091-7613(2001)029<0299:ATLPOD>2.0.CO;2)
- 1133 Peacock, S. M., & Wang, K. (2021). On the Stability of Talc in Subduction Zones: A Possible  
1134 Control on the Maximum Depth of Decoupling Between the Subducting Plate and Mantle  
1135 Wedge. *Geophysical Research Letters*, 48(17), 1–8. <https://doi.org/10.1029/2021GL094889>
- 1136 Peters, D., Bretscher, A., John, T., Scambelluri, M., & Pettke, T. (2017). Fluid-mobile elements  
1137 in serpentinites: Constraints on serpentinisation environments and element cycling in subduction  
1138 zones. *Chemical Geology*, 466(March), 654–666. <https://doi.org/10.1016/j.chemgeo.2017.07.017>
- 1139 Petriglieri, J. R., Salvioli-Mariani, E., Mantovani, L., Tribaudino, M., Lottici, P. P., Laporte-  
1140 Magoni, C., & Bersani, D. (2015). Micro-Raman mapping of the polymorphs of serpentine.  
1141 *Journal of Raman Spectroscopy*, 46(10), 953-958. <https://doi.org/10.1002/jrs.4695>
- 1142 Pirard, C., & Hermann, J. (2015). Focused fluid transfer through the mantle above subduction  
1143 zones. *Geology*, 43(10), 915–918. <https://doi.org/10.1130/G37026.1>
- 1144 Pirard, C., Hermann, J., & O'Neill, H. S. C. (2013). Petrology and Geochemistry of the Crust–  
1145 Mantle Boundary in a Nascent Arc, Massif du Sud Ophiolite, New Caledonia, SW Pacific.  
1146 *Journal of Petrology*, 54(9), 1759-1792. <https://doi.org/10.1093/petrology/egt030>
- 1147 Pirard, C., & Spandler, C. (2017). The zircon record of high-pressure metasedimentary rocks of  
1148 New Caledonia: Implications for regional tectonics of the south-west Pacific. *Gondwana  
1149 Research*, 46, 79-94. <https://doi.org/10.1016/j.gr.2017.03.001>
- 1150 Potel, S., Mählmann, R. F., Stern, W. B., Mullis, J., & Frey, M. (2006). Very Low-grade  
1151 Metamorphic Evolution of Pelitic Rocks under High-pressure/Low-temperature Conditions, NW  
1152 New Caledonia (SW Pacific). *Journal of Petrology*, 47(5), 991–1015.  
1153 <https://doi.org/10.1093/petrology/egl001>
- 1154 Prinzhofer, A., 1981. Structure et pétrologie d'un cortège ophiolitique: le massif du Sud  
1155 (Nouvelle Calédonie). Ph.D. thesis. Ecole Nationale Supérieure des Mines de Paris.

- 1156 Prinzhofer, A., & Nicolas, A. (1980). The Bogota Peninsula, New Caledonia: A Possible  
1157 Oceanic Transform Fault. *The Journal of Geology*, 88(4), 387–398.  
1158 <https://doi.org/10.1086/628523>
- 1159 Prinzhofer, A., & Allègre, C. J. (1985). Residual peridotites and the mechanisms of partial  
1160 melting. *Earth and Planetary Science Letters*, 74(2–3), 251–265. [https://doi.org/10.1016/0012-  
1161 821X\(85\)90025-1](https://doi.org/10.1016/0012-821X(85)90025-1)
- 1162 Proctor, B., & Hirth, G. (2015). Role of pore fluid pressure on transient strength changes and  
1163 fabric development during serpentine dehydration at mantle conditions: Implications for  
1164 subduction-zone seismicity. *Earth and Planetary Science Letters*, 421, 1–12.  
1165 <https://doi.org/10.1016/j.epsl.2015.03.040>
- 1166 Ranero, C. R., Phipps Morgan, J., McIntosh, K., & Reichert, C. (2003). Bending-related faulting  
1167 and mantle serpentinization at the Middle America trench. *Nature*, 425(6956), 367–373.  
1168 <https://doi.org/10.1038/nature01961>
- 1169 Rawling, T. J., & Lister, G. S. (2002). Large-scale structure of the eclogite–blueschist belt of  
1170 New Caledonia. *Journal of Structural Geology*, 24(8), 1239–1258.  
1171 [https://doi.org/10.1016/S0191-8141\(01\)00128-6](https://doi.org/10.1016/S0191-8141(01)00128-6)
- 1172 Reynard, B. (2013). Serpentine in active subduction zones. *Lithos*, 178, 171–185.  
1173 <https://doi.org/10.1016/j.lithos.2012.10.012>
- 1174 Ribeiro, J. M., & Lee, C.-T. A. (2017). An imbalance in the deep water cycle at subduction  
1175 zones: The potential importance of the fore-arc mantle. *Earth and Planetary Science Letters*, 479,  
1176 298–309. <https://doi.org/10.1016/j.epsl.2017.09.018>
- 1177 Rouméjon, S., Cannat, M., Agrinier, P., Godard, M., & Andreani, M. (2015). Serpentinization  
1178 and Fluid Pathways in Tectonically Exhumed Peridotites from the Southwest Indian Ridge (62-  
1179 65 E). *Journal of Petrology*, 56(4), 703–734. <https://doi.org/10.1093/petrology/egv014>

- 1180 Rüpke, L. H., Morgan, J. P., Hort, M., & Connolly, J. A. (2004). Serpentine and the subduction  
1181 zone water cycle. *Earth and Planetary Science Letters*, 223(1–2), 17–34.  
1182 <https://doi.org/10.1016/j.epsl.2004.04.018>
- 1183 Saccocia, P. J., Seewald, J. S., & Shanks, W. C. (2009). Oxygen and hydrogen isotope  
1184 fractionation in serpentine–water and talc–water systems from 250 to 450°C, 50MPa.  
1185 *Geochimica et Cosmochimica Acta*, 73(22), 6789–6804.  
1186 <https://doi.org/10.1016/j.gca.2009.07.036>
- 1187 Salters, V. J. M., & Stracke, A. (2004). Composition of the depleted mantle. *Geochemistry,*  
1188 *Geophysics, Geosystems*, 5(5). <https://doi.org/10.1029/2003GC000597>
- 1189 Savov, I. P., Ryan, J. G., D’Antonio, M., & Fryer, P. (2007). Shallow slab fluid release across  
1190 and along the Mariana arc-basin system: Insights from geochemistry of serpentinized peridotites  
1191 from the Mariana fore arc. *Journal of Geophysical Research*, 112(B9), B09205.  
1192 <https://doi.org/10.1029/2006JB004749>
- 1193 Savov, I. P., Ryan, J. G., D’Antonio, M., Kelley, K., & Mattie, P. (2005). Geochemistry of  
1194 serpentinized peridotites from the Mariana Forearc Conical Seamount, ODP Leg 125:  
1195 Implications for the elemental at subduction zones. *Geochemistry, Geophysics, Geosystems*,  
1196 6(4). <https://doi.org/10.1029/2004GC000777>
- 1197 Scambelluri, M., Strating, E. H. H., Piccardo, G. B., Vissers, R. L. M., & Rampone, E. (1991).  
1198 Alpine olivine- and titanian clinohumite-bearing assemblages in the Erro-Tobbio peridotite  
1199 (Voltri Massif, NW Italy). *Journal of Metamorphic Geology*, 9(1), 79–91.  
1200 <https://doi.org/10.1111/j.1525-1314.1991.tb00505.x>
- 1201 Scambelluri, M., Cannà, E., & Gilio, M. (2019). The water and fluid-mobile element cycles  
1202 during serpentinite subduction. A review. *European Journal of Mineralogy*, 31(3), 405–428.  
1203 <https://doi.org/10.1127/ejm/2019/0031-2842>

- 1204 Scambelluri, M., Fiebig, J., Malaspina, N., Müntener, O., & Pettke, T. (2004). Serpentinite  
1205 Subduction: Implications for Fluid Processes and Trace-Element Recycling. *International*  
1206 *Geology Review*, 46(7), 595–613. <https://doi.org/10.2747/0020-6814.46.7.595>
- 1207 Scambelluri, M., & Tonarini, S. (2012). Boron isotope evidence for shallow fluid transfer across  
1208 subduction zones by serpentinized mantle. *Geology*, 40(10), 907–910.  
1209 <https://doi.org/10.1130/G33233.1>
- 1210 Schmidt, M. W., & Poli, S. (1998). Experimentally based water budgets for dehydrating slabs  
1211 and consequences for arc magma generation. *Earth and Planetary Science Letters*, 163(1–4),  
1212 361–379. [https://doi.org/10.1016/S0012-821X\(98\)00142-3](https://doi.org/10.1016/S0012-821X(98)00142-3)
- 1213 Schwartz, S., Allemand, P., & Guillot, S. (2001). Numerical model of the effect of serpentinites  
1214 on the exhumation of eclogitic rocks: insights from the Monviso ophiolitic massif (Western  
1215 Alps). *Tectonophysics*, 342(1-2), 193-206. [https://doi.org/10.1016/S0040-1951\(01\)00162-7](https://doi.org/10.1016/S0040-1951(01)00162-7)
- 1216 Schwartz, S., Gautheron, C., Ketcham, R. A., Brunet, F., Corre, M., Agranier, A., et al. (2020).  
1217 Unraveling the exhumation history of high-pressure ophiolites using magnetite (U-Th-Sm)/He  
1218 thermochronometry. *Earth and Planetary Science Letters*, 543, 116359.  
1219 <https://doi.org/10.1016/j.epsl.2020.116359>
- 1220 Secchiari, A., Gleissner, P., Li, C., Goncharov, A., Milke, R., Becker, H., et al. (2020). Highly  
1221 siderophile and chalcophile element behaviour in abyssal-type and supra-subduction zone  
1222 mantle: New insights from the New Caledonia ophiolite. *Lithos*, 354–355(December 2019),  
1223 105338. <https://doi.org/10.1016/j.lithos.2019.105338>
- 1224 Secchiari, A., Montanini, A., Bosch, D., Macera, P., & Cluzel, D. (2016). Melt extraction and  
1225 enrichment processes in the New Caledonia lherzolites: Evidence from geochemical and Sr–Nd  
1226 isotope data. *Lithos*, 260(May), 28–43. <https://doi.org/10.1016/j.lithos.2016.04.030>
- 1227 Secchiari, A., Montanini, A., Bosch, D., Macera, P., & Cluzel, D. (2018). The contrasting  
1228 geochemical message from the New Caledonia gabbro-norites: insights on depletion and

- 1229 contamination processes of the sub-arc mantle in a nascent arc setting. *Contributions to*  
1230 *Mineralogy and Petrology*, 173(8), 66. <https://doi.org/10.1007/s00410-018-1496-8>
- 1231 Sécher, D. (1981). *Les lherzolites ophiolitiques de Nouvelle-Calédonie et leurs gisements de*  
1232 *chromite*. L'Institut des Sciences de la Nature de L'Université de Nantes.
- 1233 Sharp, Z. D., Atudorei, V., & Durakiewicz, T. (2001). A rapid method for determination of  
1234 hydrogen and oxygen isotope ratios from water and hydrous minerals. *Chemical Geology*,  
1235 178(1–4), 197–210. [https://doi.org/10.1016/S0009-2541\(01\)00262-5](https://doi.org/10.1016/S0009-2541(01)00262-5)
- 1236 Sharp, Z. D. (1990). A laser-based microanalytical method for the in situ determination of  
1237 oxygen isotope ratios of silicates and oxides. *Geochimica et Cosmochimica Acta*, 54(5), 1353–  
1238 1357. [https://doi.org/10.1016/0016-7037\(90\)90160-M](https://doi.org/10.1016/0016-7037(90)90160-M)
- 1239 Shen, T., Hermann, J., Zhang, L., Lü, Z., Padrón-Navarta, J. A., Xia, B., & Bader, T. (2015).  
1240 UHP Metamorphism Documented in Ti-chondrodite- and Ti-clinohumite-bearing Serpentinized  
1241 Ultramafic Rocks from Chinese Southwestern Tianshan. *Journal of Petrology*, 56(7), 1425-1458.  
1242 <https://doi.org/10.1093/petrology/egv042>
- 1243 Shimoda, G., & Kogiso, T. (2019). Effect of Serpentinite Dehydration in Subducting Slabs on  
1244 Isotopic Diversity in Recycled Oceanic Crust and Its Role in Isotopic Heterogeneity of the  
1245 Mantle. *Geochemistry, Geophysics, Geosystems*, 20(11), 5449–5472.  
1246 <https://doi.org/10.1029/2019GC008336>
- 1247 Spandler, C., Hermann, J., Faure, K., Mavrogenes, J. A., & Arculus, R. J. (2008). The  
1248 importance of talc and chlorite “hybrid” rocks for volatile recycling through subduction zones;  
1249 evidence from the high-pressure subduction mélange of New Caledonia. *Contributions to*  
1250 *Mineralogy and Petrology*, 155(2), 181-198. <https://doi.org/10.1007/s00410-007-0236-2>
- 1251 Spandler, C., Rubatto, D., & Hermann, J. (2005). Late Cretaceous-Tertiary tectonics of the  
1252 southwest Pacific: Insights from U-Pb sensitive, high-resolution ion microprobe (SHRIMP)  
1253 dating of eclogite facies rocks from New Caledonia. *Tectonics*, 24(3).  
1254 <https://doi.org/10.1029/2004TC001709>

- 1255 Sun, S. -s., & McDonough, W. F. (1989). Chemical and isotopic systematics of oceanic basalts:  
1256 implications for mantle composition and processes. Geological Society, London, Special  
1257 Publications, 42(1), 313-345. <https://doi.org/10.1144/GSL.SP.1989.042.01.19>
- 1258 Sutherland, R., Dickens, G. R., Blum, P., & Scientists, the E. 371. (2019). Tasman Frontier  
1259 Subduction Initiation and Paleogene Climate (R. Sutherland, G. R. Dickens, & P. Blum, Eds.).  
1260 Proceedings of the International Ocean Discovery Program, 371: College Station, TX  
1261 (International Ocean Discovery Program). <https://doi.org/10.14379/iodp.proc.371.2019>
- 1262 Taetz, S., John, T., Bröcker, M., & Spandler, C. (2016). Fluid–rock interaction and evolution of a  
1263 high-pressure/low-temperature vein system in eclogite from New Caledonia: insights into  
1264 intraslab fluid flow processes. *Contributions to Mineralogy and Petrology*, 171(11), 90.  
1265 <https://doi.org/10.1007/s00410-016-1295-z>
- 1266 Taetz, S., John, T., Bröcker, M., Spandler, C., & Stracke, A. (2018). Fast intraslab fluid-flow  
1267 events linked to pulses of high pore fluid pressure at the subducted plate interface. *Earth and*  
1268 *Planetary Science Letters*, 482, 33–43. <https://doi.org/10.1016/j.epsl.2017.10.044>
- 1269 Tarling, M. S., Rooney, J. S., Viti, C., Smith, S. A. F., & Gordon, K. C. (2018). Distinguishing  
1270 the Raman spectrum of polygonal serpentine. *Journal of Raman Spectroscopy*, 49(12), 1978–  
1271 1984. <https://doi.org/10.1002/jrs.5475>
- 1272 Tatsumi, Y. (1986). Formation of the volcanic front in subduction zones. *Geophysical Research*  
1273 *Letters*, 13(8), 717-720. <https://doi.org/10.1029/GL013i008p00717>
- 1274 Tenthorey, E., & Hermann, J. (2004). Composition of fluids during serpentinite breakdown in  
1275 subduction zones: Evidence for limited boron mobility. *Geology*, 32(10), 865.  
1276 <https://doi.org/10.101130/G20610.1>
- 1277 Tewksbury-Christle, C. M., Behr, W. M., & Helper, M. A. (2021). Tracking Deep Sediment  
1278 Underplating in a Fossil Subduction Margin: Implications for Interface Rheology and Mass and  
1279 Volatile Recycling. *Geochemistry, Geophysics, Geosystems*, 22(3), 1–32.  
1280 <https://doi.org/10.1029/2020GC009463>

- 1281 Toffol, G., Yang, J., Pennacchioni, G., Faccenda, M., & Scambelluri, M. (2022). How to quake a  
1282 subducting dry slab at intermediate depths: Inferences from numerical modelling. *Earth and*  
1283 *Planetary Science Letters*, 578, 117289. <https://doi.org/10.1016/j.epsl.2021.117289>
- 1284 Ulmer, P., & Trommsdorff, V. (1995). Serpentine Stability to Mantle Depths and Subduction-  
1285 Related Magmatism. *Science*, 268(5212), 858–861. <https://doi.org/10.1126/science.268.5212.858>
- 1286 Ulrich, M., Muñoz, M., Boulvais, P., Cathelineau, M., Cluzel, D., Guillot, S., & Picard, C.  
1287 (2020). Serpentinization of New Caledonia peridotites: from depth to (sub-)surface.  
1288 *Contributions to Mineralogy and Petrology*, 175(9), 91. [https://doi.org/10.1007/s00410-020-](https://doi.org/10.1007/s00410-020-01713-0)  
1289 [01713-0](https://doi.org/10.1007/s00410-020-01713-0)
- 1290 Ulrich, M., Picard, C., Guillot, S., Chauvel, C., Cluzel, D., & Meffre, S. (2010). Multiple melting  
1291 stages and refertilization as indicators for ridge to subduction formation: The New Caledonia  
1292 ophiolite. *Lithos*, 115(1–4), 223–236. <https://doi.org/10.1016/j.lithos.2009.12.011>
- 1293 Valley, J. W., Kitchen, N., Kohn, M. J., Niendorf, C. R., & Spicuzza, M. J. (1995). UWG-2, a  
1294 garnet standard for oxygen isotope ratios: Strategies for high precision and accuracy with laser  
1295 heating. *Geochimica et Cosmochimica Acta*, 59(24), 5223-5231. [https://doi.org/10.1016/0016-](https://doi.org/10.1016/0016-7037(95)00386-X)  
1296 [7037\(95\)00386-X](https://doi.org/10.1016/0016-7037(95)00386-X)
- 1297 van Keken, P. E., Hacker, B. R., Syracuse, E. M., & Abers, G. A. (2011). Subduction factory: 4.  
1298 Depth-dependent flux of H<sub>2</sub>O from subducting slabs worldwide. *Journal of Geophysical*  
1299 *Research*, 116(B1), B01401. <https://doi.org/10.1029/2010JB007922>
- 1300 Vitale Brovarone, A., & Agard, P. (2013). True metamorphic isograds or tectonically sliced  
1301 metamorphic sequence? New high-spatial resolution petrological data for the New Caledonia  
1302 case study. *Contributions to Mineralogy and Petrology*, 166(2), 451-469.  
1303 <https://doi.org/10.1007/s00410-013-0885-2>
- 1304 Vitale Brovarone, A., Agard, P., Monié, P., Chauvet, A., & Rabaute, A. (2018). Tectonic and  
1305 metamorphic architecture of the HP belt of New Caledonia. *Earth-Science Reviews*,  
1306 178(January), 48-67. <https://doi.org/10.1016/j.earscirev.2018.01.006>

1307 Wada, I., Wang, K., He, J., & Hyndman, R. D. (2008). Weakening of the subduction interface  
1308 and its effects on surface heat flow, slab dehydration, and mantle wedge serpentinization. *Journal*  
1309 *of Geophysical Research*, 113(B4), B04402. <https://doi.org/10.1029/2007JB005190>

1310 Wakabayashi, J. (1992). Nappes, Tectonics of Oblique Plate Convergence, and Metamorphic  
1311 Evolution Related to 140 Million Years of Continuous Subduction, Franciscan Complex,  
1312 California. *The Journal of Geology*, 100(1), 19–40. <https://doi.org/10.1086/629569>

1313 Whitney, D. L., & Evans, B. W. (2010). Abbreviations for names of rock-forming  
1314 minerals. *American Mineralogist*, 95(1), 185-187.

1315 Wu, K., Ding, X., Ling, M.-X., Sun, W., Zhang, L.-P., Hu, Y.-B., & Huang, R.-F. (2018).  
1316 Origins of two types of serpentinites from the Qinling orogenic belt, central China and associated  
1317 fluid/melt-rock interactions. *Lithos*, 302-303, 50-64. <https://doi.org/10.1016/j.lithos.2017.12.019>

1318 Wunder, B., & Schreyer, W. (1997). Antigorite: High-pressure stability in the system  
1319  $\text{MgO} \square \text{SiO}_2 \square \text{H}_2\text{O}$  (MSH). *Lithos*, 41(1–3), 213–227. [https://doi.org/10.1016/S0024-](https://doi.org/10.1016/S0024-4937(97)82013-0)  
1320 [4937\(97\)82013-0](https://doi.org/10.1016/S0024-4937(97)82013-0)

1321 **Figure 1.** Schematic subduction zone cross-section showing relevant locations of  
1322 serpentinization and enrichments and loss of fluid-mobile elements during subduction and  
1323 exhumation (after Deschamps et al., 2013; Peters et al., 2017). Large semi-transparent arrow  
1324 indicates subduction and exhumation path of serpentinites, emphasizing that these rocks can  
1325 encounter chemical changes on both the prograde and retrograde paths. Subduction zone after  
1326 Guillot et al. (2015).

1327 **Figure 2.** (a) Regional map highlighting significant tectonic features of the SW Pacific region  
1328 after Maurizot & Collot (2009) and Sutherland et al. (2019). (b) Simplified geologic map of the  
1329 main island of New Caledonia showing sample locations and additional localities referenced in  
1330 text. Map and units after Maurizot et al. (2020c). (c) Simplified map of Pam Peninsula showing  
1331 locations of Group I serpentinites samples (this study) and prior studied samples. Unit names  
1332 after Maurizot et al. (2020c) and boundaries modified after Vitale-Brovarone et al. (2018). (d)  
1333 Simplified map showing sampled locations at Poadja Massif. Estimated uncertainty for

1334 Fitzherbert et al. (2004) georeferenced raster map locations (c, d) is ~500-700 m and ~200-400  
1335 m, respectively. Solid black lines denote roads, solid blue lines denote streams, and dashed black  
1336 line denotes high-angle normal fault.

1337 **Figure 3.** Backscatter electron images from select high-pressure serpentinites. (a) A relict  
1338 chromite core surrounded by a mantle of ferritchromite and rim of chromian magnetite  
1339 containing inclusions of antigorite (NC19-48). (b) Delicate veins of tremolite and antigorite cross  
1340 cut a pervasively serpentinized matrix (NC19-94). (c) Skeletal chromite replaced by magnetite  
1341 and antigorite (NC18-39B). (d) Inclusions of Fe-Ni alloy awaruite and antigorite in magnetite  
1342 (NC18-39A). (e) Brightness-contrast enhanced image highlighting complex curvilinear  
1343 retrogression of chromian magnetite to magnetite (NC19-154A). (f) Representative texture of  
1344 typical replacement of olivine by antigorite and magnetite via growth from fractures (NC18-  
1345 39A).

1346 **Figure 4.** Whole rock major element ratios of  $MgO/SiO_2$  vs.  $Al_2O_3/SiO_2$  for serpentinites and  
1347 hybrid rocks in New Caledonia's HP/LT terrane. Samples are plotted with compiled data for  
1348 harzburgites in the New Caledonia ophiolite (gray circles) (Liu et al., 2018; Mothersole, 2014;  
1349 Mothersole et al., 2017; Ulrich et al., 2010). Also shown is the field for abyssal serpentinites  
1350 from Niu (2004). Depleted mantle value from McDonough and Sun (1995), primitive mantle  
1351 value from Salters and Stracke (2004). "Terrestrial array" line after Hart and Zindler (1986),  
1352 Jagoutz et al. (1979), and Niu (2004).

1353 **Figure 5.** Whole rock trace and REE compositions for New Caledonia HP/LT serpentinites.  
1354 Samples are plotted together (a, b) and separately into respective categories: Group I (c, d) and  
1355 Group II (e, f). Trace element concentrations are normalized to primitive mantle values of Sun  
1356 and McDonough (1989) (a,c,e). REE concentrations are normalized to C1 chondrite  
1357 (McDonough & Sun, 1995) (b,d,f).

1358 **Figure 6.** (a) Hydrogen ( $\delta D$ ) and oxygen ( $\delta^{18}O$ ) stable isotope compositions of New Caledonia  
1359 HP/LT serpentinites compared with existing data for serpentine in the overlying Peridotite Nappe  
1360 (ophiolite groups after Cluzel et al., 2020; Ulrich et al., 2020). Weathered samples and samples  
1361 for which antigorite was not specified in Cluzel et al. (2020) were excluded. Upper mantle values

1362 from Eiler (2001), Kyser and O'Neil (1984), and Matthey et al. (1994). (b)  $\delta^{18}\text{O}$  versus loss on  
1363 ignition (LOI) for HP/LT serpentinites. Group I serpentinites show decreasing  $\delta^{18}\text{O}$  with  
1364 progressive hydration whereas Group II serpentinites exhibit a narrow range of  $\delta^{18}\text{O}$  values  
1365 irrespective of degree of hydration. An arrow denotes the direction of  $\delta^{18}\text{O}$  change when  
1366 serpentine is formed at increasing temperatures in equilibrium with seawater (e.g., Saccocia et  
1367 al., 2009).

1368 **Figure 7.** Representative cross-polarized photomicrographs and correlated Raman spectra for (a)  
1369 two separate matrix sites in Group I sample NC18-09B and (b) one pseudomorph (red) and one  
1370 vein (blue) in Group II sample NC19-152. Diagnostic Raman peaks for antigorite are highlighted  
1371 tan vertical bars. All serpentine polymorphs in Group I and II were identified as antigorite  
1372 (Figures S5, S6).

1373 **Figure 8.** Variations in ratios of HFSE/HREE (i.e., Yb) with increasing LOI (%) for New  
1374 Caledonia HP/LT serpentinites. Variations in trace element ratios are independent of LOI value.

1375 **Figure 9.** Plots of LREE (La, Ce, Pr, and Nd) versus HFSE (e.g., Zr) for all HP/LT serpentinites,  
1376 with zoomed insets in upper right of graphs to highlight trace element depleted Group II samples.  
1377 Groups I and II symbols are the same as Figure 8. One sample, NC19-158 (open orange circle),  
1378 has been excluded from the trendline and computed R values.

1379 **Figure 10.** Plots for investigation of FME trends among New Caledonia HP/LT serpentinites.  
1380 Data are plotted against compilations for mid-ocean ridge (MOR) serpentinites (teal circles) and  
1381 forearc (FA) serpentinites (tan circles) from Peters et al. (2017). (a) Ba/Yb vs. Ba, (b) Cs/Yb vs.  
1382 Cs, (c) U vs. Th, and (d) Cs vs. Yb.

1383 **Figure 11.** REE compositions for New Caledonia HP/LT serpentinites. (a) Group I serpentinites  
1384 plotted versus a global dataset of mid-ocean ridge serpentinites (Peters et al., 2017); (b) Group II  
1385 serpentinites plotted versus harzburgite compositions from the New Caledonia ophiolite  
1386 (Marchesi et al., 2009; Secchiari et al., 2020; Ulrich et al., 2010).

Figure 1.

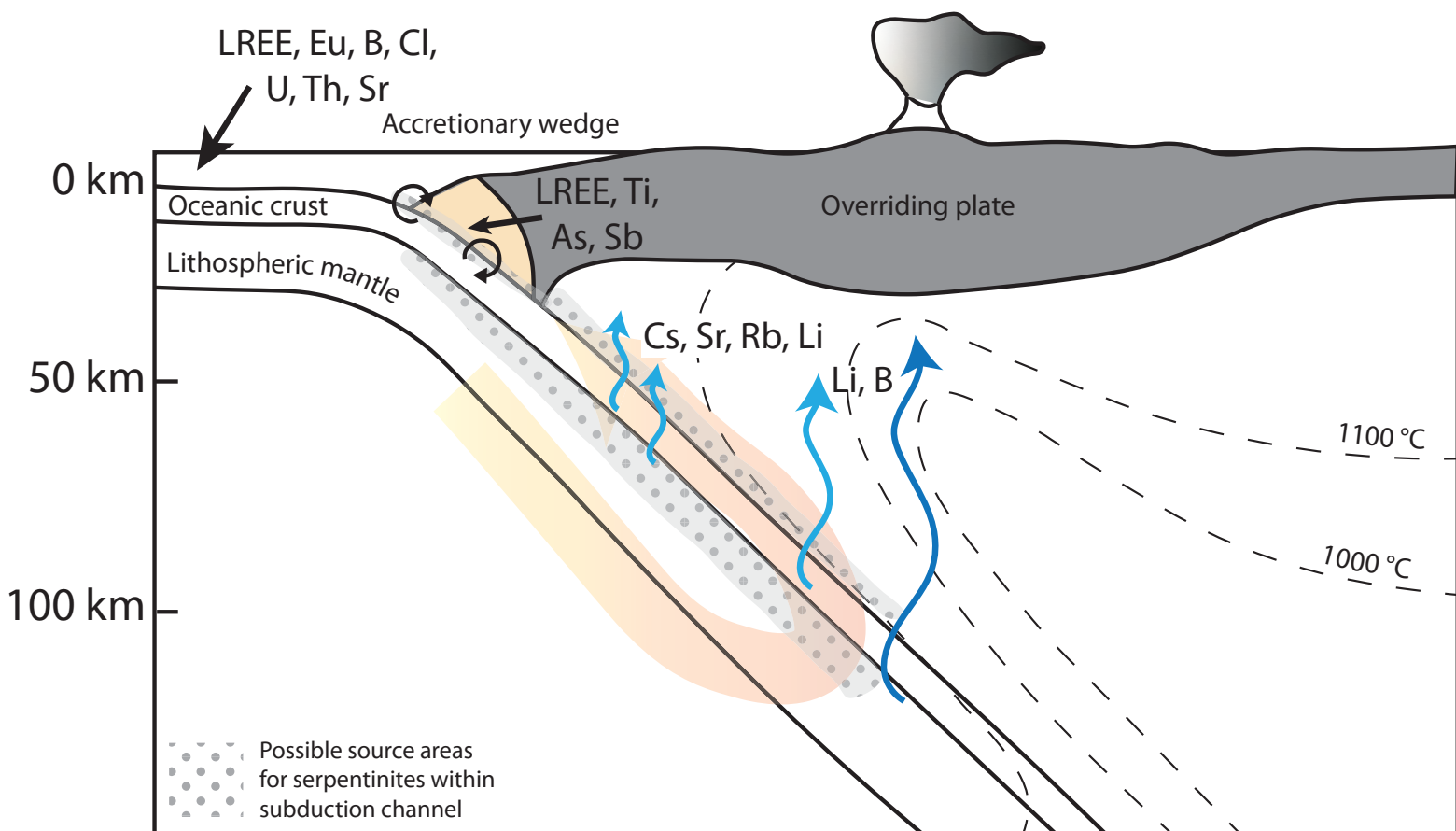


Figure 2.

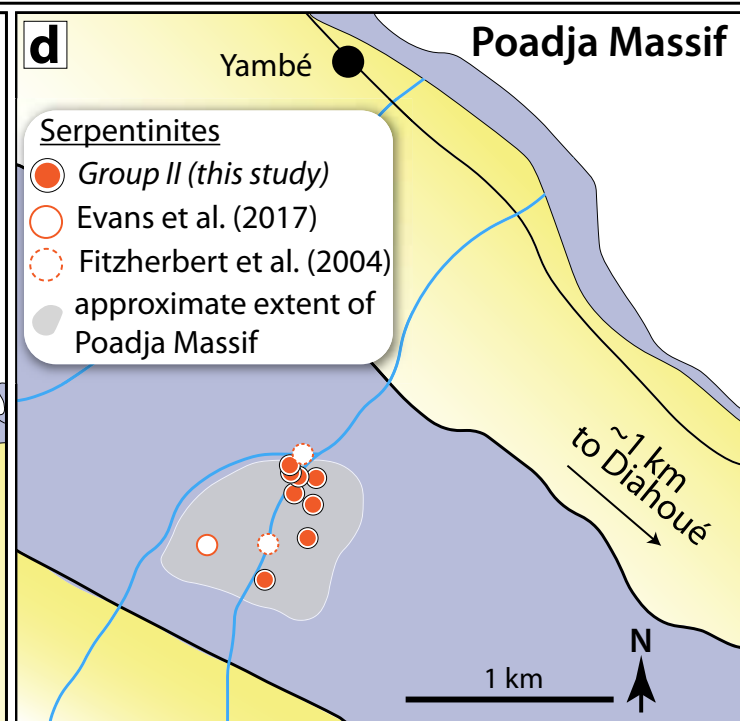
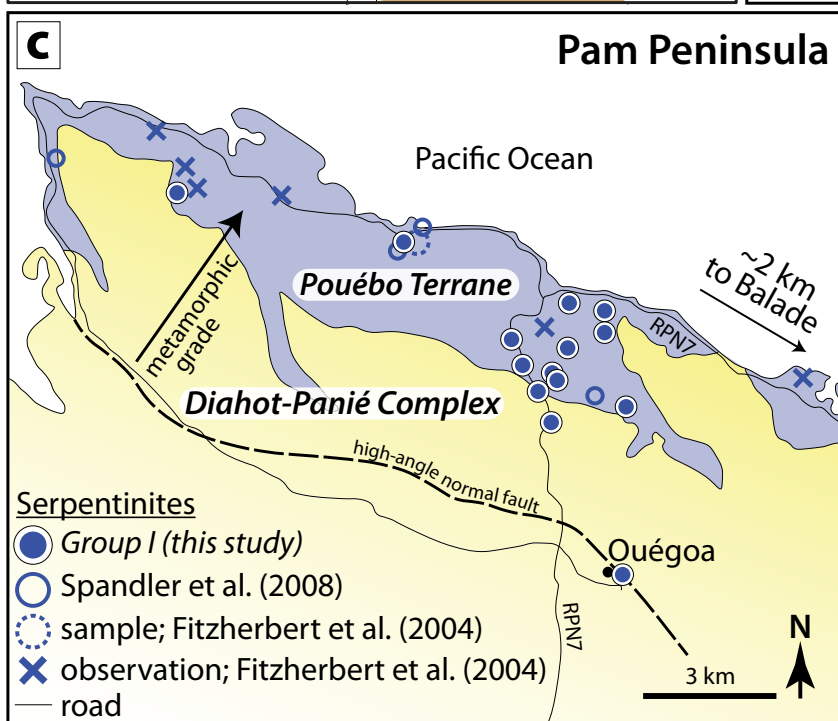
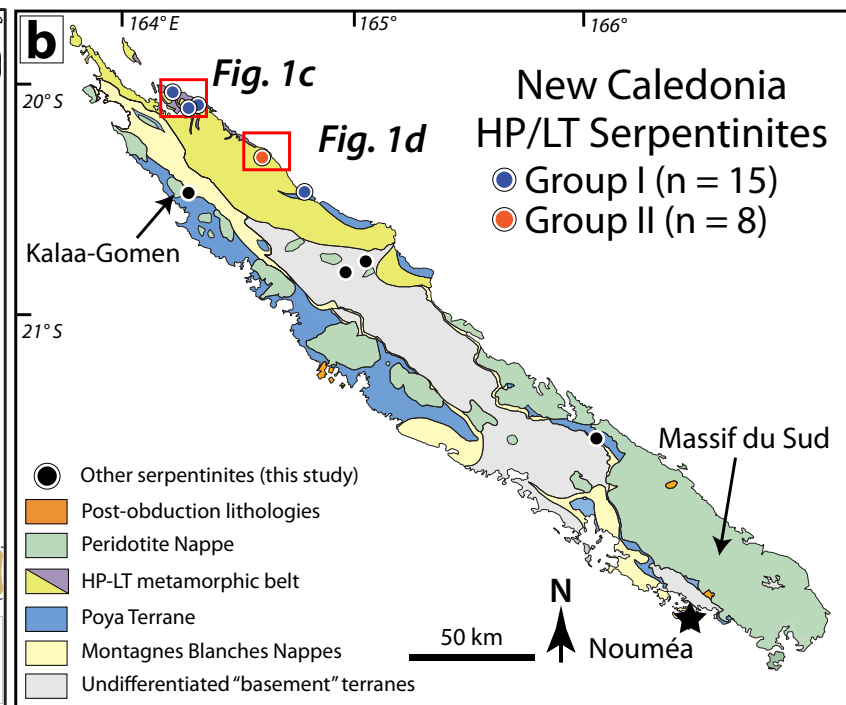
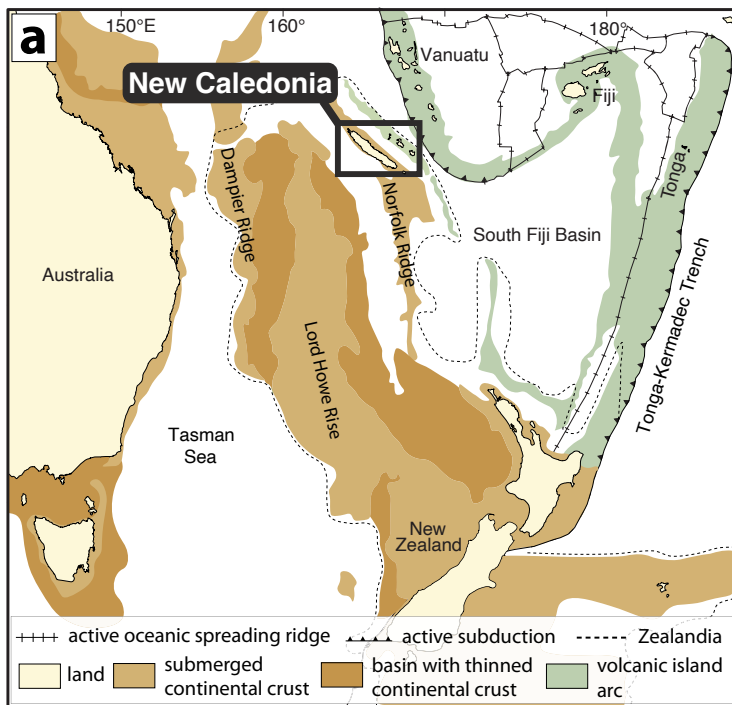


Figure 3.

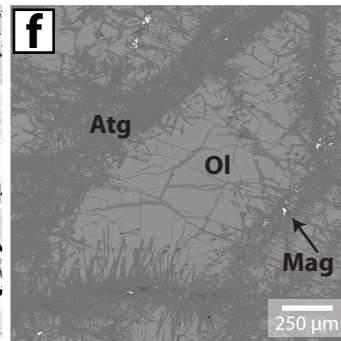
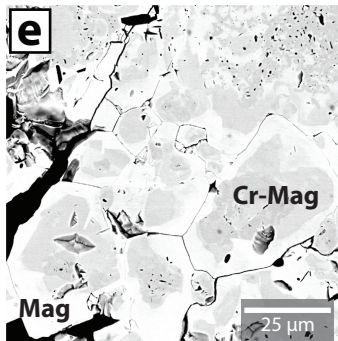
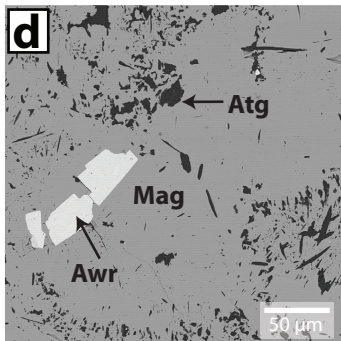
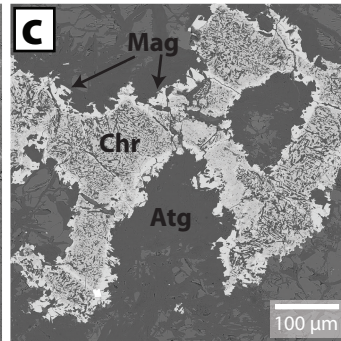
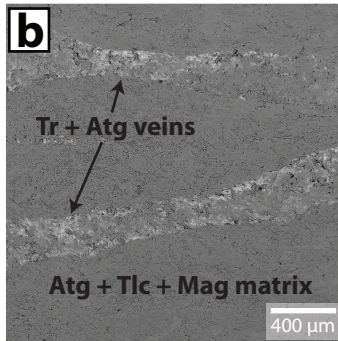
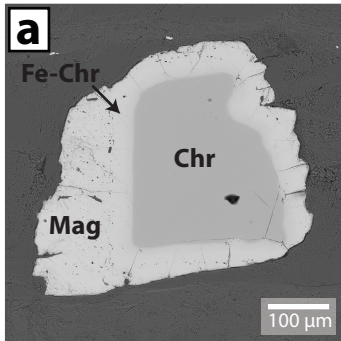


Figure 4.

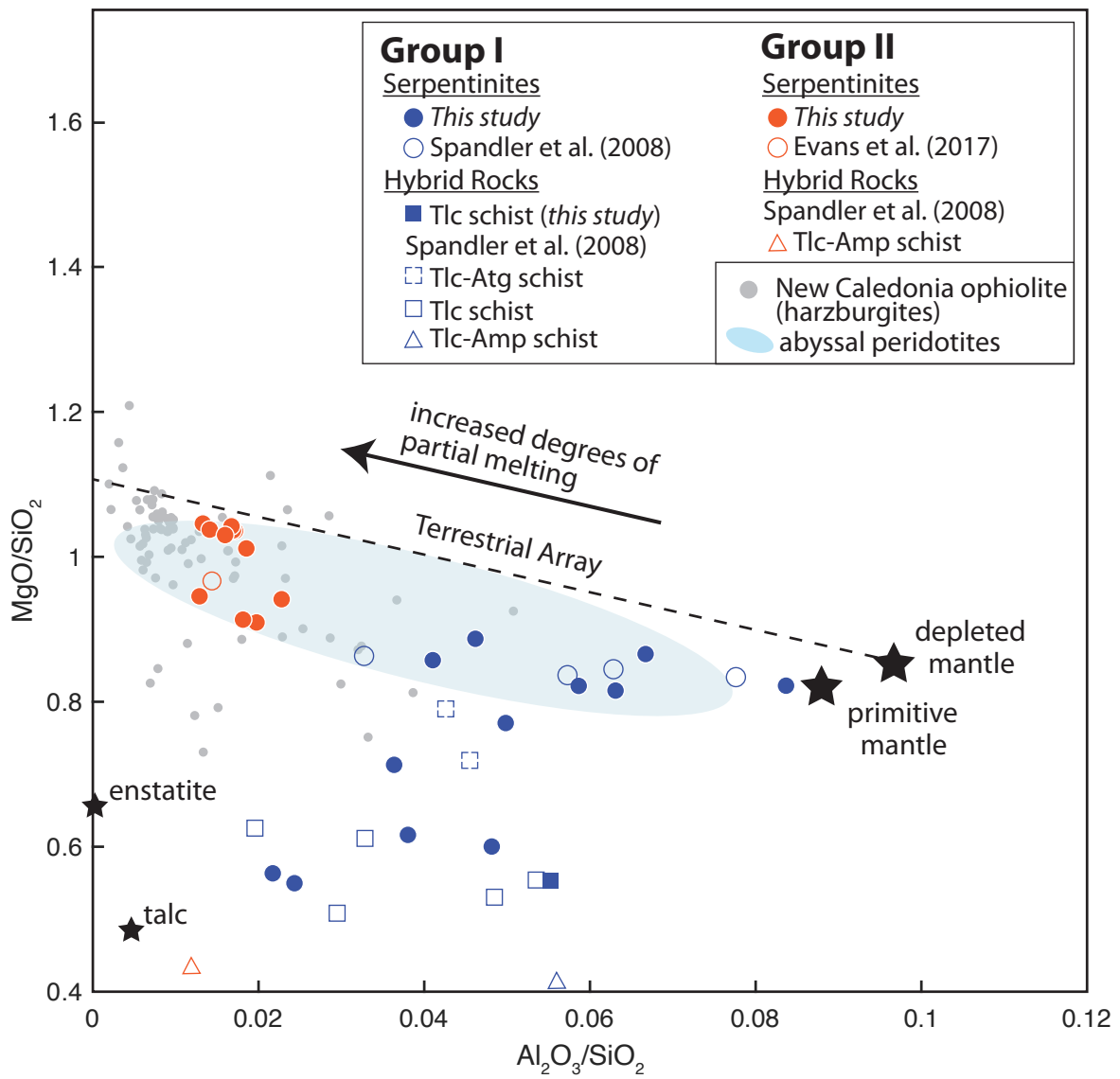


Figure 5.

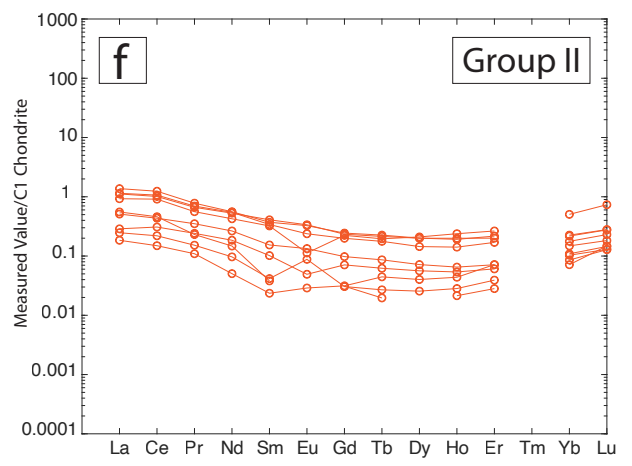
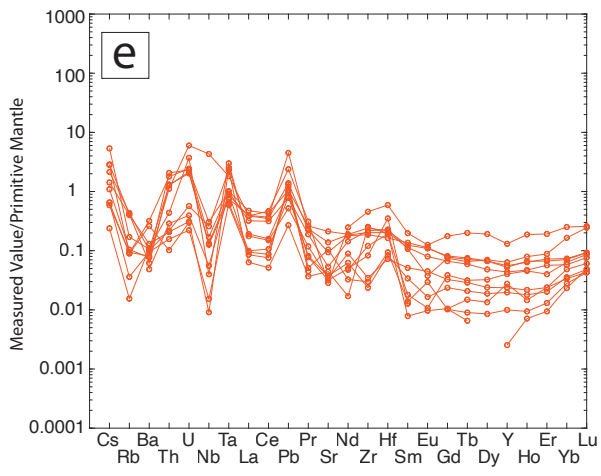
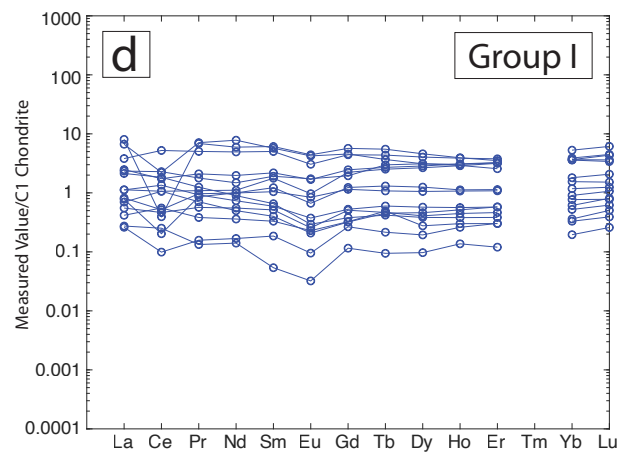
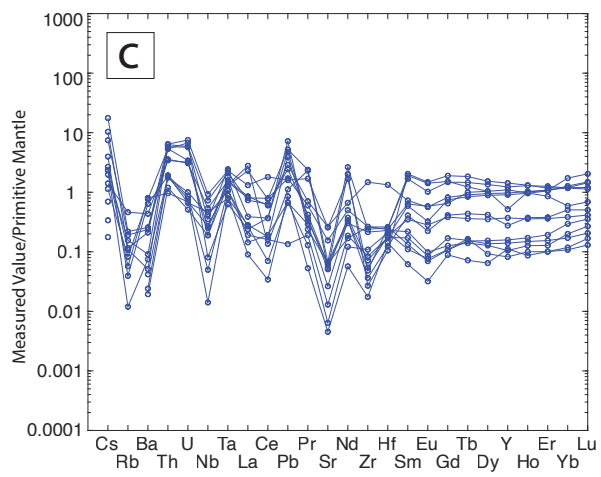
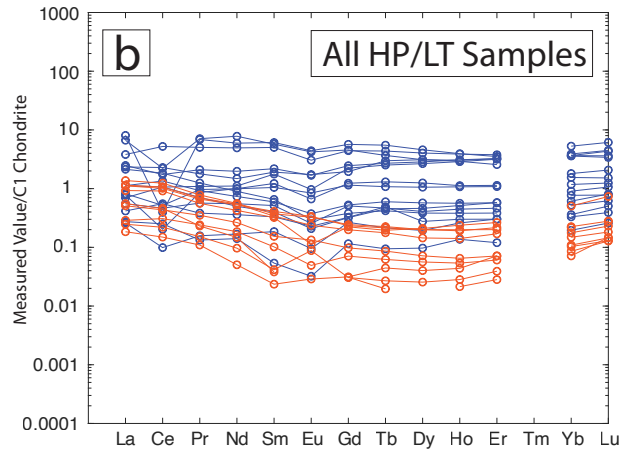
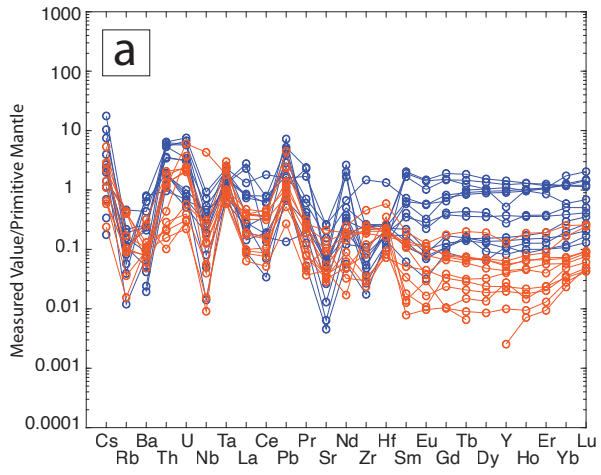


Figure 6.

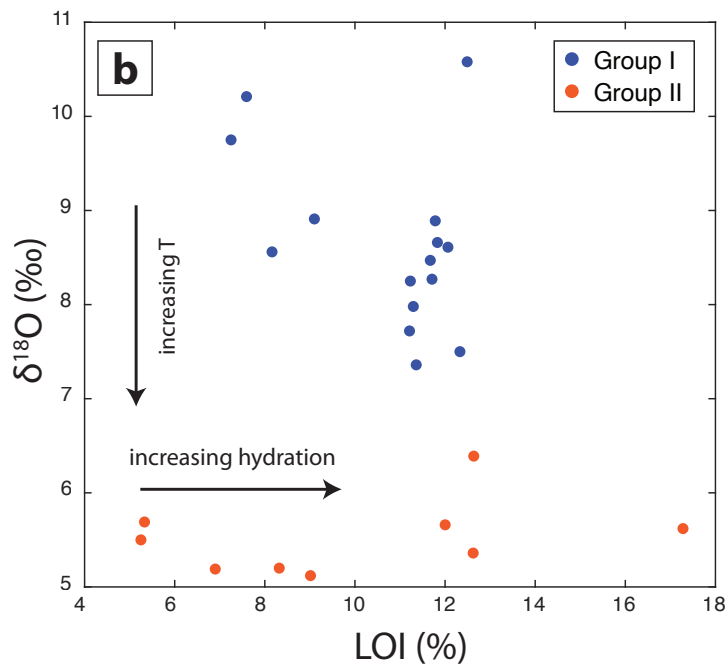
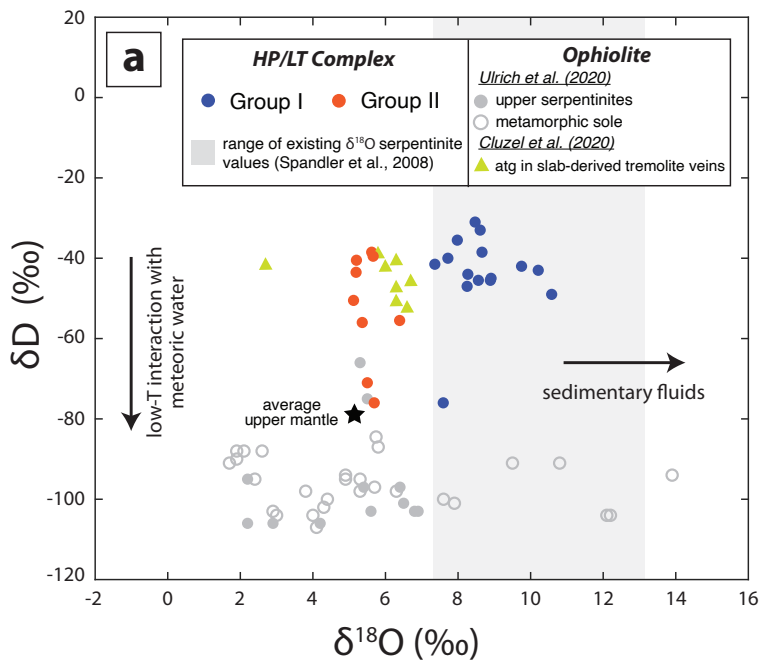


Figure 7.

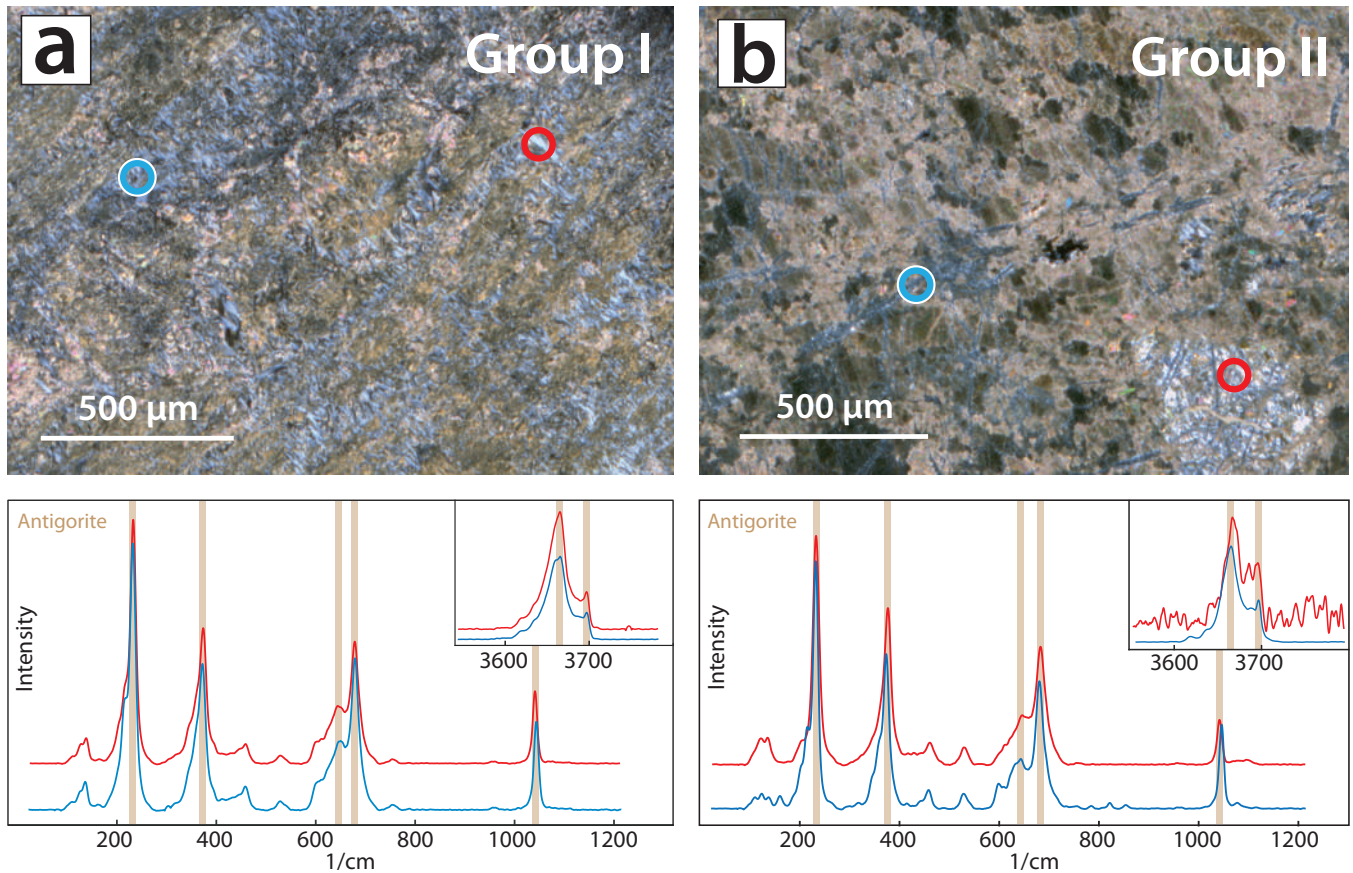


Figure 7. Representative cross-polarized photomicrographs and correlated Raman spectra for (a) two separate matrix sites in Group I sample NC18-09B and (b) one pseudomorph (red) and one vein (blue) in Group II sample NC19-152. Diagnostic Raman peaks for antigorite are highlighted tan vertical bars. All serpentine polymorphs in Group I and II were identified as antigorite (Figure S5).

Figure 8.

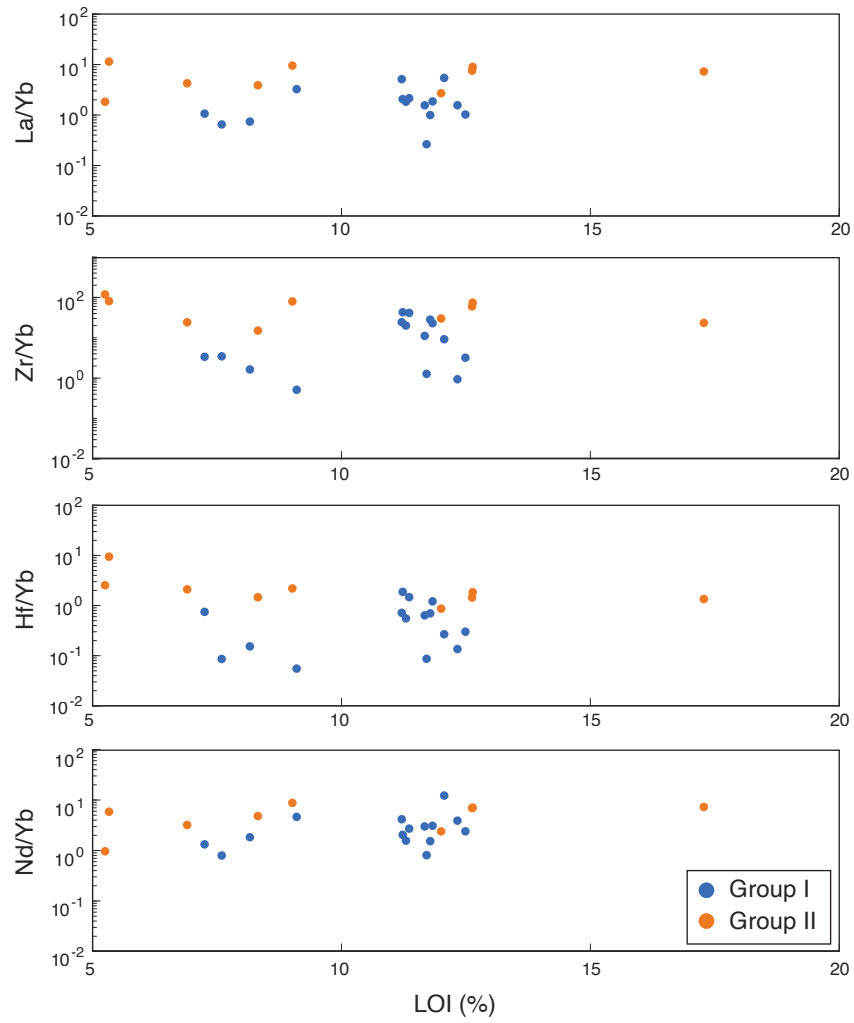


Figure 9.

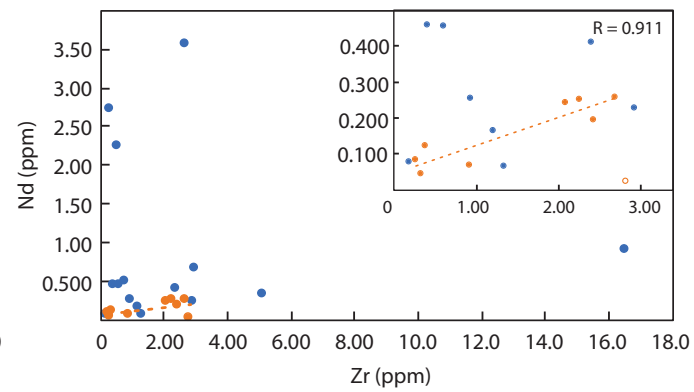
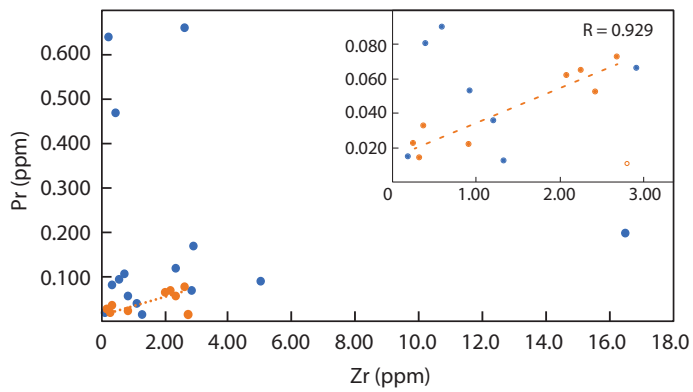
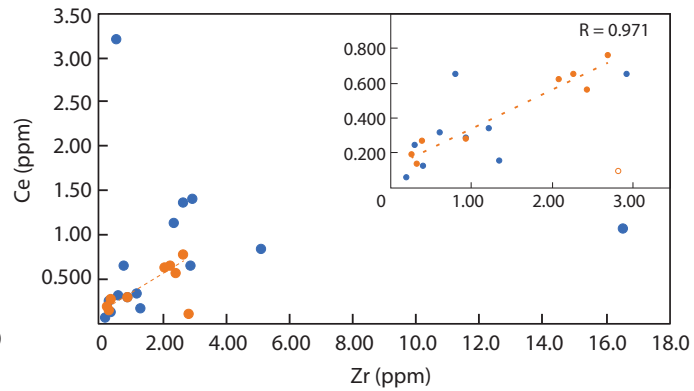
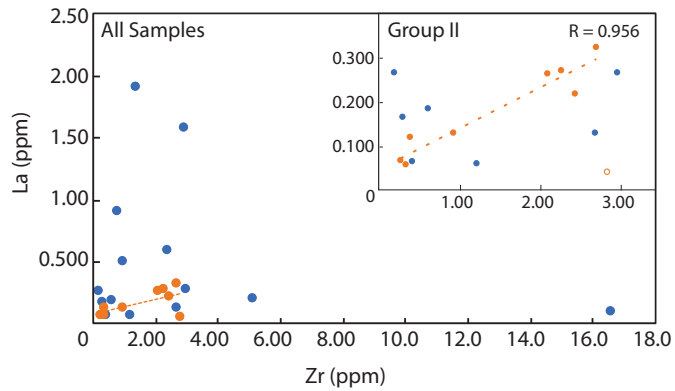


Figure 10.

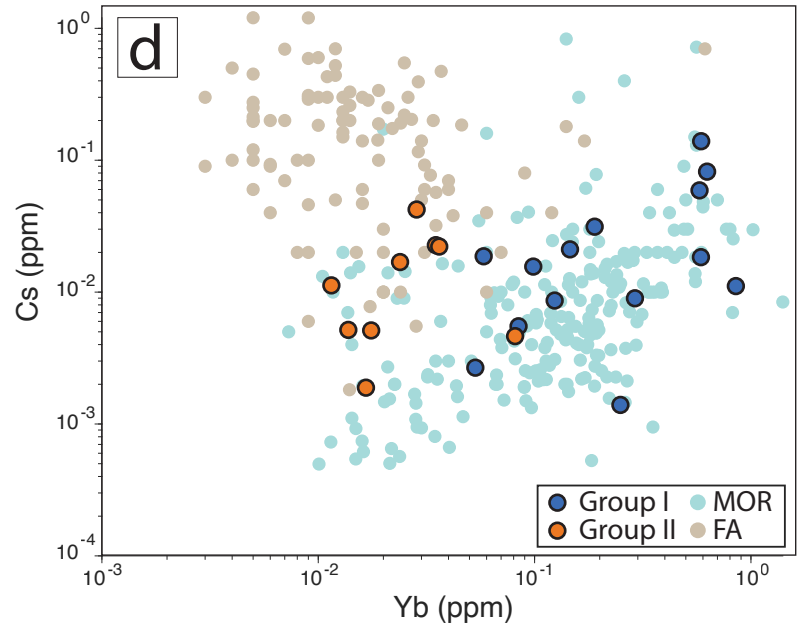
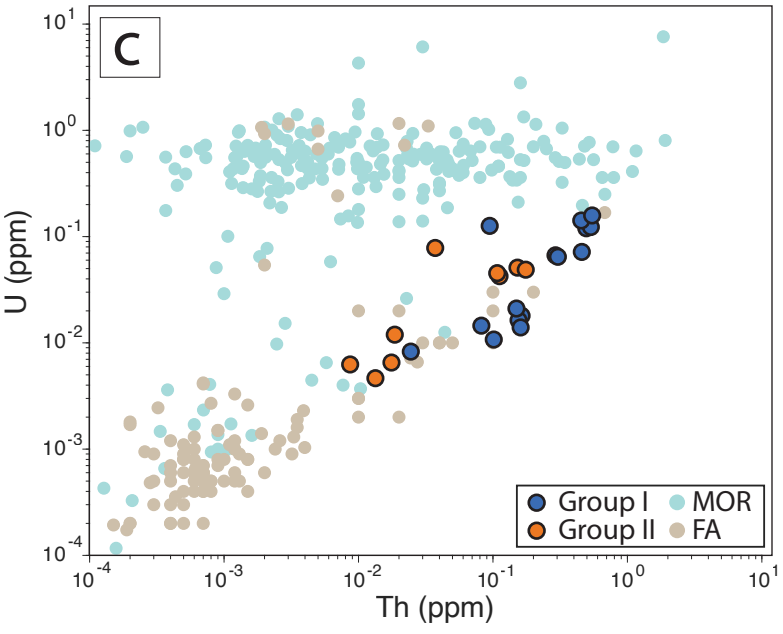
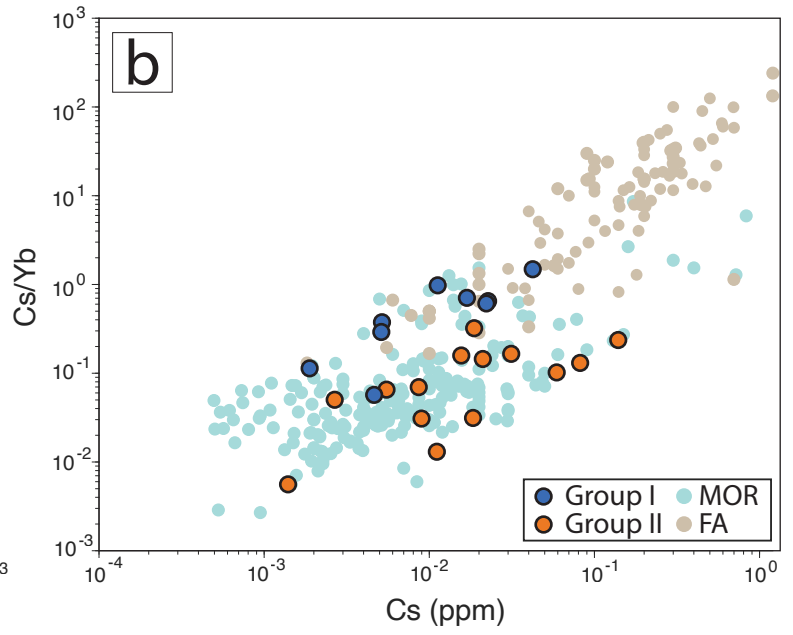
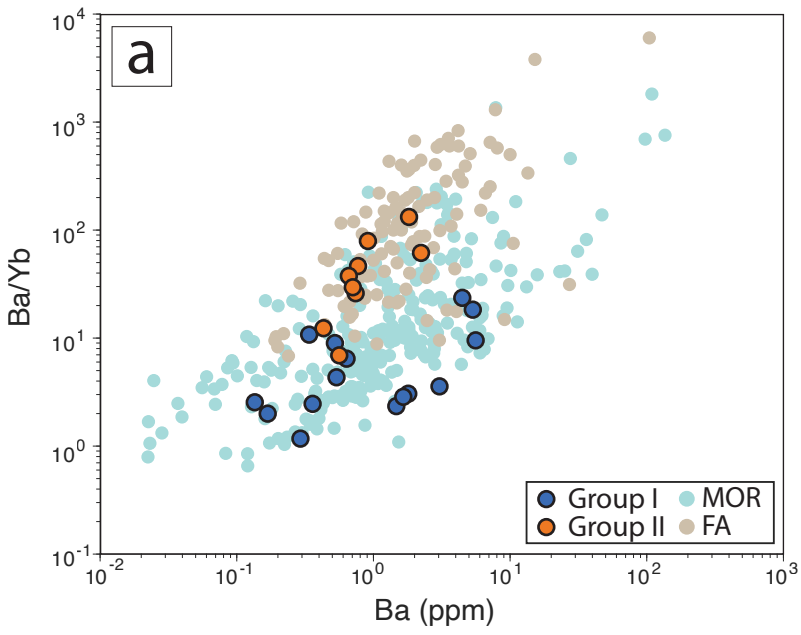
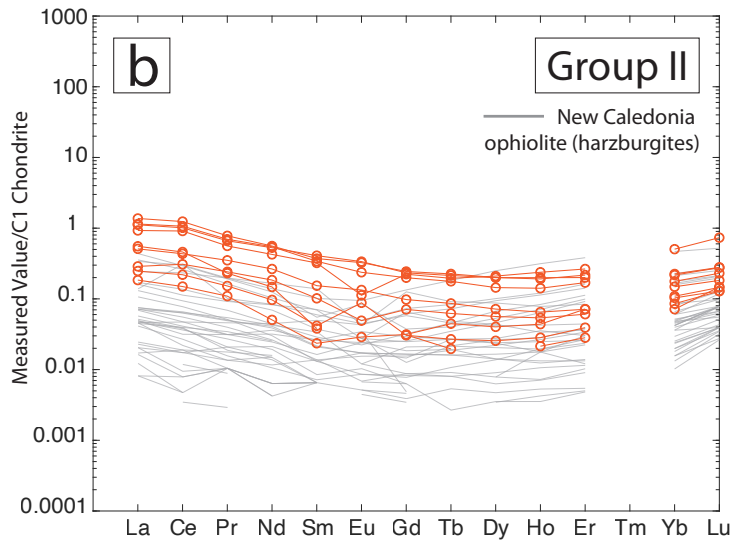
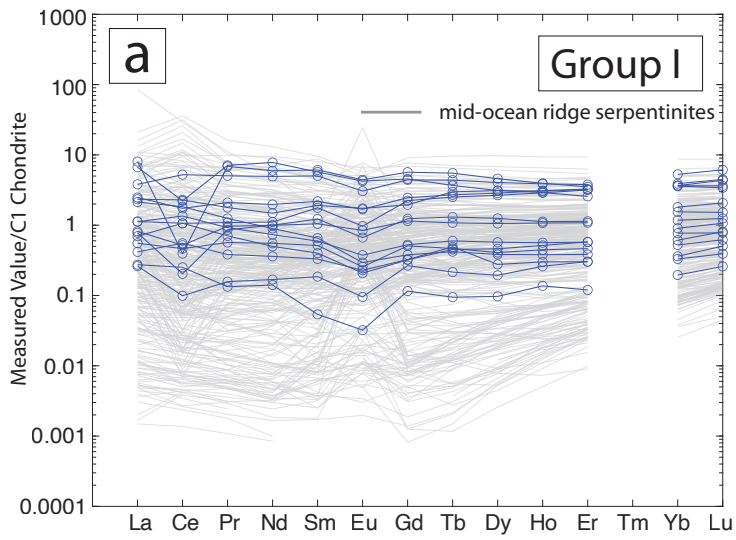


Figure 11.



**Table 1****Whole rock major and trace element compositions**

<b>Lithology</b>	<b>Serpentinite</b>				
<b>Sample name</b>	NC18-07C	NC18-09B	NC18-15C	NC18-15D	NC18-22A
<b>IGSN</b>	IENHR0002	IENHR0003	IENHR0004	IENHR0005	IENHR0006
<b>Group/Locality</b>	I	I	I	I	I
<b>Major elements (wt%)</b>					
SiO <sub>2</sub>	53.95	43.78	41.90	42.25	41.32
TiO <sub>2</sub>	0.02	0.02	0.02	0.02	0.02
Al <sub>2</sub> O <sub>3</sub>	1.31	2.18	2.46	1.73	3.46
Fe <sub>2</sub> O <sub>3(T)</sub>	6.39	8.56	8.63	7.50	9.63
MnO	0.04	0.11	0.16	0.10	0.14
MgO	29.65	33.74	34.44	36.22	33.97
CaO	0.03	0.02	0.01	<0.01	0.01
Na <sub>2</sub> O	0.00	0.00	0.00	<0.01	<0.01
K <sub>2</sub> O	0.01	0.00	0.00	<0.01	<0.01
P <sub>2</sub> O <sub>5</sub>	0.01	0.00	0.01	<0.01	<0.01
LOI <sup>a</sup>	7.59	11.30	12.06	11.67	11.21
Total	98.98	99.69	99.68	99.50	99.76
Mg#	0.82	0.80	0.80	0.83	0.78
Lab	WSU	WSU	WSU	WSU	WSU
<b>Trace elements (ppm)</b>					
Li	n.d.	n.d.	n.d.	0.0464	n.d.
Be	n.d.	n.d.	n.d.	0.110	n.d.
Sc	7.12	10.4	8.33	7.97	11.5
V	n.d.	n.d.	n.d.	37.3	n.d.
Cr	n.d.	n.d.	n.d.	2252	n.d.
Co	n.d.	n.d.	n.d.	94.8	n.d.
Ni	n.d.	n.d.	n.d.	2384	n.d.
Cu	n.d.	n.d.	n.d.	1.89	n.d.
Zn	n.d.	n.d.	n.d.	29.4	n.d.
Ga	n.d.	n.d.	n.d.	2.73	n.d.
Rb	0.293	0.0691	0.0525	bdl	0.0992
Sr	3.27	1.34	1.43	0.274	1.29
Y	2.36	0.720	4.99	0.637	0.478
Zr	2.95	2.93	2.68	0.938	2.40
Nb	0.180	0.251	0.136	0.0356	0.519
Cs	0.0111	0.0211	0.00898	0.00551	0.0156
Ba	3.04	0.359	5.33	0.168	0.636

La	0.554	0.267	1.58	0.131	0.506
Ce	1.40	0.653	1.36	0.285	1.12
Pr	0.165	0.0655	0.659	0.0526	0.116
Nd	0.677	0.228	3.57	0.253	0.410
Sm	0.283	0.0592	0.845	0.0761	0.0970
Eu	0.0977	0.0117	0.238	0.0144	0.0165
Tb	0.108	0.0163	0.133	0.0168	0.0151
Gd	0.388	0.0638	0.906	0.101	0.0755
Dy	0.765	0.113	0.765	0.100	0.0943
Ho	0.166	0.0281	0.159	0.0244	0.0208
Er	0.515	0.0925	0.411	0.0742	0.0614
Tm	0.102	0.0169	0.0533	0.0122	0.0117
Yb	0.852	0.146	0.291	0.0843	0.0986
Lu	0.151	0.0262	0.0509	0.0152	0.0199
Hf	0.0733	0.0808	0.0779	0.0538	0.0705
Ta	0.0605	0.0998	0.0528	0.0443	0.0864
Pb	0.121	0.512	0.371	0.00955	0.173
Th	0.292	0.495	0.458	0.163	0.534
U	0.0667	0.120	0.0717	0.0180	0.123
Lab	WSU	WSU	WSU	URI	WSU

*Note* . n.d. = not determined; bdl = below detection limits; F&M = Franklin & Marshall College; URI = aLOI measured by combustion

NC18-26B IENHR0008 	NC18-43 IENHR000C 	NC19-14 IENHR000G 	NC19-48 IENHR000I 	NC19-54 IENHR000J 	NC19-63 IENHR000K 	NC19-81 IENHR000L 
38.46	46.20	42.45	54.34	42.52	42.48	51.51
0.22	0.01	0.01	0.01	0.01	0.01	<0.01
6.73	1.68	1.96	1.18	0.84	2.68	2.48
13.39	7.00	6.50	6.30	7.09	8.29	6.83
0.14	0.07	0.10	0.07	0.09	0.12	0.07
29.19	32.94	37.65	30.61	38.67	34.64	30.92
0.44	0.11	0.01	0.02	0.01	0.02	0.14
<0.01	0.18	0.03	0.01	0.03	0.02	0.02
<0.01	0.02	<0.01	<0.01	<0.01	<0.01	<0.01
<0.01	<0.01	<0.01	<0.01	<0.01	<0.01	<0.01
11.78	12.33	11.83	7.25	11.36	12.49	8.16
100.35	100.54	100.54	99.79	100.62	100.75	100.13
0.69	0.82	0.85	0.83	0.85	0.81	0.82
WSU	F&M	F&M	F&M	F&M	F&M	F&M
n.d.	5.72	0.0154	0.907	1.75	2.08	0.820
n.d.	0.846	0.0985	0.155	0.126	0.236	0.0904
13.8	10.5	6.72	4.03	6.71	11.5	7.75
n.d.	43.0	27.8	25.2	33.7	41.2	45.4
n.d.	2400	2500	2193	2861	2280	2103
n.d.	88.8	91.9	88.0	169	69.6	82.1
n.d.	2209	2299	2368	5877	1942	2288
n.d.	4.09	4.61	2.98	17.1	24.6	2.12
n.d.	39.4	35.9	40.9	106	34.0	34.7
n.d.	4.51	2.00	1.98	1.83	3.18	3.31
0.139	0.122	bdl	0.00760	0.0662	0.0250	bdl
5.54	5.40	0.135	0.0957	0.602	1.39	0.558
4.41	5.59	0.374	0.507	0.595	1.69	1.26
16.6	0.543	1.22	0.196	5.11	0.609	0.409
0.384	0.661	0.134	0.0100	3.07	0.331	0.296
0.139	0.0591	0.00267	0.0187	0.00863	0.0313	0.00140
1.80	1.65	0.135	0.522	0.537	4.47	0.292

0.587	0.903	0.0988	0.0619	0.266	0.194	0.185
1.07	3.21	0.339	0.0607	0.827	0.317	0.124
0.195	0.468	0.0355	0.0146	0.0857	0.0896	0.0798
0.902	2.26	0.165	0.0770	0.336	0.455	0.457
0.323	0.744	0.0489	0.0274	0.0878	0.155	0.181
0.0947	0.172	0.0129	0.00537	0.0211	0.0475	0.0375
0.0975	0.158	0.0177	0.00776	0.0216	0.0390	0.0472
0.489	0.881	0.0646	0.0530	0.105	0.228	0.246
0.702	0.994	0.0680	0.0477	0.141	0.260	0.308
0.169	0.211	0.0164	0.0142	0.0307	0.0586	0.0614
0.520	0.604	0.0482	0.0485	0.0921	0.173	0.182
0.0849	0.0911	0.00814	0.00799	0.0169	0.0268	0.0323
0.589	0.579	0.0532	0.0581	0.124	0.189	0.249
0.107	0.0837	0.00963	0.0124	0.0191	0.0306	0.0374
0.411	0.0786	0.0645	0.0436	0.182	0.0570	0.0382
0.0639	0.0939	0.0745	0.0362	0.0744	0.0322	0.0434
0.204	0.114	0.0482	0.0606	0.169	0.278	0.0475
0.304	0.547	0.101	0.155	0.0946	0.161	0.149
0.0646	0.158	0.0107	0.0163	0.126	0.0140	0.0210
WSU	URI	URI	URI	URI	URI	URI

= University of Rhode Island; WSU = Washington State University.

NC19-86 IENHR000N I	NC19-89 IENHR000O I	NC19-94 IENHR000P I	NC18-39A (core) IENHR0009 II	NC18-39A (rxn) IENHR0009 II	NC18-39B IENHR000A II
41.69	50.75	42.12	38.57	40.64	40.05
0.02	0.01	0.01	0.01	0.01	0.01
0.95	1.93	2.81	0.51	0.52	0.57
7.15	7.10	7.50	7.49	7.29	7.59
0.05	0.09	0.13	0.11	0.12	0.11
39.25	31.28	36.47	40.34	38.42	41.55
0.03	0.02	0.06	<0.01	0.17	0.57
0.03	<0.01	0.03	<0.01	<0.01	<0.01
<0.01	<0.01	<0.01	<0.01	<0.01	<0.01
0.01	<0.01	<0.01	<0.01	<0.01	<0.01
11.23	9.10	11.71	12.62	12.64	9.01
100.41	100.28	100.84	99.66	99.81	99.46
0.85	0.82	0.83	0.84	0.84	0.85
F&M	F&M	F&M	WSU	WSU	WSU
0.0470	0.602	1.60	n.d.	n.d.	n.d.
0.0267	0.124	0.326	n.d.	n.d.	n.d.
8.03	10.7	9.49	6.68	7.12	7.12
30.4	45.2	58.0	n.d.	n.d.	n.d.
2454	2747	2796	n.d.	n.d.	n.d.
52.5	93.9	110	n.d.	n.d.	n.d.
1601	2386	2678	n.d.	n.d.	n.d.
3.68	11.9	0.604	n.d.	n.d.	n.d.
30.0	42.3	40.8	n.d.	n.d.	n.d.
1.33	3.64	4.44	n.d.	n.d.	n.d.
bdl	0.0364	0.0736	0.264	0.0577	0.108
bdl	1.13	1.07	1.99	4.47	2.92
0.183	6.48	4.13	0.238	0.254	0.198
1.35	0.302	0.799	2.09	2.69	2.26
0.0397	0.194	0.0574	0.0947	0.122	0.0900
bdl	0.0184	0.0819	0.0227	0.0222	0.0423
0.339	5.59	1.47	0.431	2.23	0.741

0.0649	1.91	0.165	0.265	0.325	0.271
0.154	0.242	0.652	0.620	0.760	0.654
0.0124	0.637	0.101	0.0616	0.0723	0.0646
0.0643	2.72	0.507	0.242	0.256	0.250
0.00798	0.903	0.262	0.0605	0.0550	0.0503
0.00181	0.249	0.0545	0.0190	0.0183	0.0134
0.00341	0.198	0.0909	0.00773	0.00814	0.00639
0.0230	1.13	0.444	0.0464	0.0485	0.0396
0.0239	1.13	0.655	0.0491	0.0493	0.0355
0.00747	0.215	0.158	0.0109	0.0104	0.00772
0.0192	0.563	0.507	0.0320	0.0347	0.0272
0.00424	0.0848	0.0867	0.00475	0.00558	0.00478
0.0315	0.587	0.627	0.0350	0.0362	0.0285
0.00637	0.0891	0.110	0.00679	0.00687	0.00567
0.0592	0.0325	0.0544	0.0505	0.0669	0.0624
0.0377	0.0546	0.0257	0.0356	0.0416	0.0308
0.0841	0.0793	0.340	0.0981	0.0745	0.320
0.0245	0.0820	0.454	0.112	0.152	0.108
0.00827	0.0145	0.142	0.0424	0.0510	0.0453
URI	URI	URI	WSU	WSU	WSU

NC18-39C IENHR000B II	NC19-42 IENHR000H II	NC19-152 IENHR000Q II	NC19-154A IENHR000R II	NC19-157 IENHR000S II	NC19-158 IENHR000T II	NC18-45 IENHR000D <b>Boghen Terrane</b>
41.61	41.96	40.80	38.86	40.64	41.98	40.26
0.01	<0.01	<0.01	<0.01	<0.01	<0.01	0.01
0.75	0.72	0.69	0.72	0.68	0.67	0.41
7.21	7.75	8.28	5.75	7.55	7.91	9.41
0.09	0.11	0.12	0.09	0.11	0.11	0.15
38.01	43.46	42.29	39.31	42.35	43.24	36.43
0.01	0.50	1.08	0.02	0.42	0.53	0.01
<0.01	0.06	0.05	0.04	0.05	0.08	<0.01
<0.01	0.01	<0.01	<0.01	<0.01	0.01	<0.01
<0.01	<0.01	<0.01	<0.01	<0.01	<0.01	<0.01
12.00	5.33	6.90	17.28	8.32	5.25	13.19
99.70	99.90	100.21	102.07	100.12	99.78	99.86
0.84	0.85	0.84	0.87	0.85	0.85	0.79
WSU	F&M	F&M	F&M	F&M	F&M	WSU
n.d.	0.717	0.481	0.0560	0.180	0.630	n.d.
n.d.	bdl	bdl	0.0160	bdl	bdl	n.d.
7.20	8.75	7.01	6.74	6.01	5.39	9.79
n.d.	21.4	12.1	17.8	19.2	17.6	n.d.
n.d.	2672	1773	2285	2117	1819	n.d.
n.d.	104	97.8	98.4	103	112	n.d.
n.d.	2331	2184	2461	2278	2555	n.d.
n.d.	10.2	2.16	2.36	3.21	2.04	n.d.
n.d.	30.1	33.2	29.3	23.3	29.7	n.d.
n.d.	0.977	1.76	0.933	0.878	0.463	n.d.
0.0598	0.254	0.0568	0.00982	0.0229	0.276	0.0814
1.13	0.670	2.20	0.724	0.788	0.934	2.19
0.289	0.0115	0.0454	0.108	0.0895	0.126	0.197
2.43	0.929	0.334	0.388	0.264	2.82	2.06
0.219	0.00648	bdl	0.0284	0.0109	0.185	0.0892
0.00464	0.0112	0.00517	0.00189	0.00512	0.0169	0.0921
0.562	0.911	1.82	0.772	0.661	0.706	3.88

0.220	0.131	0.0586	0.121	0.0682	0.0437	0.281
0.559	0.282	0.135	0.266	0.189	0.0916	0.556
0.0520	0.0214	0.0141	0.0326	0.0224	0.0102	0.0546
0.194	0.0674	0.0442	0.121	0.0844	0.0231	0.212
0.0477	0.00564	0.00616	0.0227	0.0151	0.00348	0.0367
0.00634	bdl	0.00495	0.00752	0.00277	0.00163	0.0772
0.00705	0.000708	0.000971	0.00312	0.00225	0.00161	0.00446
0.0444	0.00616	0.00608	0.0195	0.0141	0.00625	0.0273
0.0517	bdl	0.00629	0.0176	0.0139	0.00989	0.0308
0.0130	0.00117	0.00154	0.00355	0.00294	0.00239	0.00704
0.0423	0.00451	0.00627	0.0114	0.00971	0.0115	0.0230
0.00821	0.00128	0.00118	0.00187	0.00176	0.00219	0.00417
0.0813	0.0115	0.0138	0.0166	0.0176	0.0239	0.0300
0.0181	0.00363	0.00315	0.00319	0.00357	0.00449	0.00509
0.0705	0.109	0.0290	0.0224	0.0257	0.0607	0.0558
0.0403	0.105	0.0240	0.123	0.0259	0.0952	0.0311
0.0555	0.0684	0.0932	0.0369	0.0576	0.0191	0.860
0.175	0.0176	0.00867	0.0372	0.0134	0.0186	0.123
0.0488	0.00653	0.00626	0.0782	0.00465	0.0119	0.0374
WSU	URI	URI	URI	URI	URI	WSU

NC18-46	NC18-49	Peridotite NC19-178	Chlorite schist NC19-85	Talc schist NC19-169	
IENHR000E	IENHR000F	IENHR000V	IENHR000M	IENHR000U	
Boghen Terrane	Serpentinite Sole	Kalaa-Gomen	I	I	
39.00	42.04	40.51		22.35	54.16
0.02	<0.01	<0.01		3.54	0.02
1.05	0.51	0.69		13.43	2.99
10.22	6.91	7.73		29.21	6.62
0.15	0.06	0.11		0.24	0.02
36.38	37.51	40.91		19.23	29.93
<0.01	0.04	0.66		2.47	0.03
<0.01	0.03	0.05		0.01	<0.01
<0.01	<0.01	<0.01		<0.01	<0.01
0.01	<0.01	<0.01		1.88	0.01
12.90	13.67	9.77		7.88	6.25
99.72	100.77	100.43		100.24	100.03
0.78	0.84	0.84		0.40	0.82
WSU	WSU	F&M		F&M	F&M
n.d.	1.91	1.27		7.12	0.162
n.d.	0.0109	bdl		0.252	0.0814
11.8	5.60	7.30		35.9	8.51
n.d.	19.7	26.6		448	49.0
n.d.	2314	2307		284	2336
n.d.	95.5	95.7		140	93.1
n.d.	2563	2069		247	1985
n.d.	2.55	1.82		59.7	7.40
n.d.	25.3	82.9		128	43.3
n.d.	0.645	0.879		8.47	4.28
0.144	0.00673	0.0809		0.0242	0.167
1.74	0.677	0.428		36.0	2.27
0.453	1.08	0.0220		54.8	0.327
3.12	0.497	0.353		25.0	0.256
0.155	0.00694	bdl		12.7	0.0267
0.787	0.00578	0.00336		0.00499	0.0109
3.50	0.709	0.168		12.9	0.341

0.296	0.202	0.0183	13.1	0.0523
0.600	0.170	0.0501	35.7	0.192
0.0760	0.0701	0.00444	4.29	0.0302
0.350	0.330	0.0101	20.5	0.156
0.0475	0.100	0.00109	6.42	0.0523
0.0220	0.0264	bdl	1.82	0.00663
0.00897	0.0199	0.000194	1.76	0.0118
0.0493	0.143	0.00120	9.71	0.0693
0.0652	0.110	0.000929	11.4	0.0706
0.0175	0.0273	0.000413	2.30	0.0141
0.0556	0.0752	0.00259	5.50	0.0355
0.00961	0.00983	0.000758	0.662	0.00444
0.0711	0.0544	0.00955	3.44	0.0237
0.0128	0.0109	0.00254	0.453	0.00355
0.0668	0.0437	0.0224	0.738	0.0105
0.0891	0.0525	0.0217	0.641	0.0135
0.362	0.260	0.00374	0.984	0.0827
0.0939	0.0165	0.00392	3.08	0.0223
0.0368	0.00565	0.00129	0.133	0.00457
WSU	URI	URI	URI	URI

**Table 2**  
**Oxygen and hydrogen stable isotope data.**

Sample	Rock type	Group/Locality	$\delta D_{\text{srp}}$ (‰)	$\delta^{18}O_{\text{srp}}$ (‰)
NC18-07C	serpentinite	I	-45, -41	10.2
NC18-09B	serpentinite	I	-35, -36	8.0
NC18-15C	serpentinite	I	-34, -32	8.6
NC18-15D	serpentinite	I	-33, -29	8.5, 6.7
NC18-22A	serpentinite	I	-40, -40	7.7, 6.8
NC18-26B	serpentinite	I	-44, -46	8.9
NC18-43	serpentinite	I	-75, -77	7.5
NC19-14	serpentinite	I	-38, -39	8.7, 8.8
NC19-48	serpentinite	I	-42, -42	9.8
NC19-54	serpentinite	I	-42, -41	7.4, 7.2
NC19-63	serpentinite	I	-49, -49	10.6
NC19-81	serpentinite	I	-47, -44	8.6
NC19-86	serpentinite	I	-47, -47	8.3
NC19-89	serpentinite	I	-45, -45	8.9, 8.8
NC19-94	serpentinite	I	-44, -44	8.3
NC18-39A (core)	serpentinite	II	-59, -53	5.4
NC18-39A (rxn)	serpentinite	II	-56, -55	6.4
NC18-39B	serpentinite	II	-52, -49	5.1, 5.5
NC18-39C	serpentinite	II	-39, -40	5.7
NC19-42	serpentinite	II	-73, -79	5.7
NC19-152	serpentinite	II	-43, -44	5.2
NC19-154A	serpentinite	II	-40, -37	5.6
NC19-157	serpentinite	II	-42, -39	5.2
NC19-158	serpentinite	II	-70, -72	5.5
NC19-85	chlorite schist	I		
NC19-169	talc schist	I		
NC18-45	serpentinite	Boghen Terrane	-82, -86	8.0
NC18-46	serpentinite	Boghen Terrane	-78, -79	7.0
NC18-49	serpentinite	Serpentinite Sole	-82, -82	6.5
NC19-178	serpentinite	Kalaa-Gomen Massif	-84, -85	5.7

*Note.* Mineral abbreviations after Whitney and Evans (2010): *Srp* serpentine, *Mag* mag<sup>1</sup>>710  $\mu\text{m}$  grain size fraction  
<sup>2</sup> 125-250  $\mu\text{m}$  grain size fraction

$\delta^{18}\text{O}_{\text{mag}}$  (‰)

$\delta^{18}\text{O}_{\text{tlc}}$  (‰)

9.0

1.5

2.3, 2.5  
4.3<sup>1</sup>, 4.6<sup>2</sup>

10.5

agnetite, *Tlc* talc